JEM Journal of Experimental Medicine

ARTICLE

Bone marrow–derived fibroblasts are a functionally distinct stromal cell population in breast cancer

Yael Raz[1,2]*, Noam Cohen[1]*, Ophir Shani[1], Rachel E. Bell[3], Sergey V. Novitskiy[4], Lilach Abramovitz[1], Carmit Levy[3], Michael Milyavsky[1], Leonor Leider-Trejo[5], Harold L. Moses[4], Dan Grisaru[2], and Neta Erez[1]

Cancer-associated fibroblasts (CAFs) are highly prominent in breast tumors, but their functional heterogeneity and origin are still largely unresolved. We report that bone marrow (BM)–derived mesenchymal stromal cells (MSCs) are recruited to primary breast tumors and to lung metastases and differentiate to a distinct subpopulation of CAFs. We show that BM-derived CAFs are functionally important for tumor growth and enhance angiogenesis via up-regulation of Clusterin. Using newly generated transgenic mice and adoptive BM transplantations, we demonstrate that BM-derived fibroblasts are a substantial source of CAFs in the tumor microenvironment. Unlike resident CAFs, BM-derived CAFs do not express PDGFRα, and their recruitment resulted in a decrease in the percentage of PDGFRα-expressing CAFs. Strikingly, decrease in PDGFRα in breast cancer patients was associated with worse prognosis, suggesting that BM-derived CAFs may have deleterious effects on survival. Therefore, PDGFRα expression distinguishes two functionally unique CAF populations in breast tumors and metastases and may have important implications for patient stratification and precision therapeutics.

Introduction

Despite extensive research, breast cancer remains one of the leading causes of cancer-related deaths in women in the Western world. Cancer-associated fibroblasts (CAFs) are a heterogeneous population of stromal cells in the microenvironment of solid tumors. In some cancer types, including breast and pancreatic carcinomas, CAFs are the most prominent stromal cell type, and their abundance was shown to correlate with worse outcome (Tsujino et al., 2007). Nevertheless, CAFs are the least-characterized cells in the tumor microenvironment, and their origin and function in tumors continue to be a subject of debate. Moreover, the origin of CAFs in the metastatic microenvironment is unknown. CAFs were shown to promote tumor growth by stimulating cancer cell proliferation and by enhancing angiogenesis (Hanahan and Coussens, 2012). CAFs also modify extracellular matrix architecture through enhanced deposition of collagen and mediate increased cross-linking of collagen fibers, thus stiffening the stroma, which was found to correlate with tumor progression (Erler and Weaver, 2009; Levental et al., 2009; Goetz et al., 2011). CAFs were also implicated in mediating tumor-promoting inflammation via secretion of cytokines and chemokines that contribute to the recruitment of immune cells to the tumor microenvironment (Erez et al., 2010; Servais and Erez, 2013). In several tumor types, including breast cancer, pro-inflammatory activity of CAFs is induced at the earliest preneoplastic stages. Moreover, pro-inflammatory signaling by CAFs is operative in human breast and ovarian cancers (Erez et al., 2013).

CAFs are vastly heterogeneous and are comprised of several subpopulations with diverse origins, including activated myofibroblasts (characterized by α-smooth muscle actin [αSMA] expression), reprogrammed local tissue fibroblasts (Sharon et al., 2015) and adipocyte-derived CAFs (Bochet et al., 2013).

It was previously suggested that a subpopulation of stromal cells in the microenvironment of tumors are bone marrow (BM)–derived (Direkze et al., 2004; Anderberg and Pietras, 2009; Spaeth et al., 2013; Öhlund et al., 2014). Several in vitro studies demonstrated that mesenchymal stromal cells (MSCs) can differentiate to αSMA-expressing myofibroblasts following incubation with tumor cells (Shangguan et al., 2012; Peng et al., 2014). Co-injection of tumor cells with MSCs to immune deficient mice resulted in enhanced tumor growth and metastasis (Karnoub et al., 2007; Mi et al., 2011; Meleshina et al., 2015). However, the in vivo differentiation of BM-derived mesenchymal cells to CAFs in spontaneous primary tumors and metastases and their distinct functional role in breast cancer remain unexplored. To enable

[1]Department of Pathology, Sackler School of Medicine, Tel Aviv University, Tel Aviv, Israel; [2]Department of Obstetrics and Gynecology, Tel Aviv Sourasky Medical Center, Tel Aviv, Israel; [3]Department of Human Molecular Genetics and Biochemistry, Sackler School of Medicine, Tel Aviv University, Tel Aviv, Israel; [4]Department of Cancer Biology, Vanderbilt University School of Medicine and Vanderbilt-Ingram Comprehensive Cancer Center, Nashville, TN; [5]Department of Pathology, Tel Aviv Sourasky Medical Center, Tel Aviv University, Tel Aviv, Israel.

*Y. Raz and N. Cohen contributed equally to this paper; Correspondence to Neta Erez: netaerez@post.tau.ac.il.

unbiased tracking and characterization of fibroblast subpopulations in breast cancer, we performed adoptive BM transplantations in newly generated transgenic mice in which the Collagen-1α (Col1α) promoter drives the expression of a reporter gene (Pallangyo et al., 2015). We demonstrate that BM-derived MSCs are specifically recruited to breast tumors and to spontaneous lung metastases and are a substantial source of CAFs in the tumor microenvironment in a transgenic mouse model of human breast carcinogenesis. Detailed analysis of this distinct CAF population revealed that BM-derived CAFs do not express the receptor for platelet-derived growth factor α (PDGFRα), which was previously shown to be a robust marker of fibroblasts (Erez et al., 2010; Driskell et al., 2013). Consequently, recruitment of BM-derived CAFs to primary tumors and metastases resulted in a gradual decrease in PDGFRα levels, which was evident also in human breast tumors, and correlated with worse outcome. BM-derived CAFs exhibited a unique inflammatory profile depending on the location to which they were recruited and were functionally distinct from resident CAFs in their tumor-promoting functions in vivo, including more effective induction of angiogenesis mediated by up-regulation of Clusterin. Thus, our findings that PDGFRα expression distinguishes two functionally unique CAF populations may have implications for patient stratification and tailored therapeutics in breast cancer.

Results

The percentage of PDGFRα⁺ CAFs in mammary tumors and lung metastases decreases with tumor progression

To characterize the dynamic changes in the heterogeneous subpopulations of fibroblastic cells during the course of spontaneous breast cancer progression, we performed immunostaining analysis with known fibroblast markers including αSMA, FSP-1, PDGFRα, and Vimentin. Analysis was performed on tissue sections from mammary glands of MMTV-PyMT transgenic mice at distinct stages of tumor development. Results confirmed that CAFs are a heterogeneous population, composed of several subpopulations that only partially overlap (data not shown), as previously described in other mouse models (Sugimoto et al., 2006). In addition, we found a gradual increase in αSMA expression in mammary tissue of MMTV-PyMT mice, indicating that fibroblast activation correlates with tumor progression (Fig. 1, A and B). Increased αSMA was also evident by FACS analysis of intracellular staining in mammary tumors as compared with normal mammary glands (Fig. 1 C and Fig. S1 A). Notably, immunofluorescent staining of lungs from MMTV-PyMT mice bearing metastases revealed an increase in the population of αSMA⁺ CAFs in metastatic lesions, suggesting that gradual activation of CAFs with tumor progression is operative also in spontaneous lung metastases (Fig. 1, D and E). Analysis of αSMA expression in lung fibroblasts isolated from MMTV-PyMT mice with lung metastases, or from normal lungs revealed a striking increase in its expression in metastases-bearing lungs (Fig. 1 F).

PDGFRα was previously shown to be a robust marker of fibroblasts (Erez et al., 2010; Driskell et al., 2013; Sharon et al., 2013; Ruffell et al., 2014). We therefore performed co-staining of αSMA and PDGFRα in normal mammary glands or in tumor tissue. While in normal mammary glands, there were no double stained cells, and αSMA staining was mainly detected around ducts and vessel walls, activated fibroblasts in the tumor microenvironment were αSMA⁺ and PDGFRα⁺ (Fig. 1 G). Quantification of co-staining at different stages of mammary carcinogenesis revealed a significant increase in αSMA expression within the PDGFRα⁺ population, confirming that mammary PDGFRα⁺ fibroblasts undergo activation during tumor progression (Fig. 1 H and Fig. S1 B). Surprisingly, the inverse analysis revealed an unexpected decrease in the percentage of PDGFRα⁺ fibroblasts within the growing αSMA⁺ population (Fig. 1 I). Similarly, co-staining of PDGFRα and αSMA in spontaneous lung metastases indicated that only a subpopulation of αSMA⁺ CAFs were also PDGFRα⁺ (Fig. 1 J). Moreover, comparison of fibroblasts isolated from normal mammary glands (NMFs) or normal lungs (NLFs) with CAFs isolated from mammary tumors (mammary CAFs) or from metastases-bearing lungs (lung CAFs) confirmed that while there was an increase in the percentage of αSMA⁺ cells, the percentage of PDGFRα⁺ fibroblasts decreases in cancerous tissue (Fig. 1, K–N). To quantify this finding, we used Col1α as an unbiased marker for fibroblasts (Kalluri and Zeisberg, 2006; Pallangyo et al., 2015) and analyzed by FACS the expression of PDGFRα in fibroblasts from normal mammary tissue compared with tumor tissue. Analysis indicated that >80% of fibroblasts in normal mammary tissue express PDGFRα, while in tumor tissue, less than half (~45%) of the CAFs express PDGFRα (Fig. 1 O and Fig. S1 C). This decrease was evident also in a temporal analysis of the percentage of PDGFRα⁺ cells within CD45⁻ cells in mammary tumor tissue, while the total number of PDGFRα⁺ cells during tumor progression remained unchanged (Fig. 1, P and Q). Interestingly, the decrease in PDGFRα⁺ cells was evident in tumor tissues, but not at earlier preneoplastic stages (Fig. S1 D). Collectively, these observations suggest that in addition to the population of resident PDGFRα⁺ CAFs, there is a distinct subpopulation of PDGFRα⁻ CAFs. Intrigued by these observations, we set out to further characterize their origin and function.

A subpopulation of CAFs in mammary tumors and lung metastases is BM-derived

Based on previous studies, we hypothesized that the BM may be a source for the subpopulation of PDGFRα⁻ CAFs (Anderberg and Pietras, 2009; Öhlund et al., 2014). To test this hypothesis, we performed adoptive BM transplantations from donor mice that express GFP ubiquitously (β-actin-GFP) into MMTV-PyMT recipients. To ascertain the correct physiological background of donors and adjust for tumor-related changes, we postulated that the BM of age-matched MMTV-PyMT mice would be most appropriate and therefore generated β-actin-GFP-PyMT double transgenic mice and used them as BM donors (rather than nontransgenic mice). BM from β-actin-GFP or β-actin-GFP-PyMT female mice was transplanted into lethally irradiated nontransgenic controls (FVB/n mice) or PyMT recipients, respectively (Fig. 2 A). Control mice that were irradiated but not transplanted with BM died within 2 wk of irradiation. Importantly, irradiation did not affect disease course in MMTV-PyMT mice. Transplanted mice were monitored until tumors reached end-stage. Age-matched normal BM recipients were euthanized at the same time point. Analysis

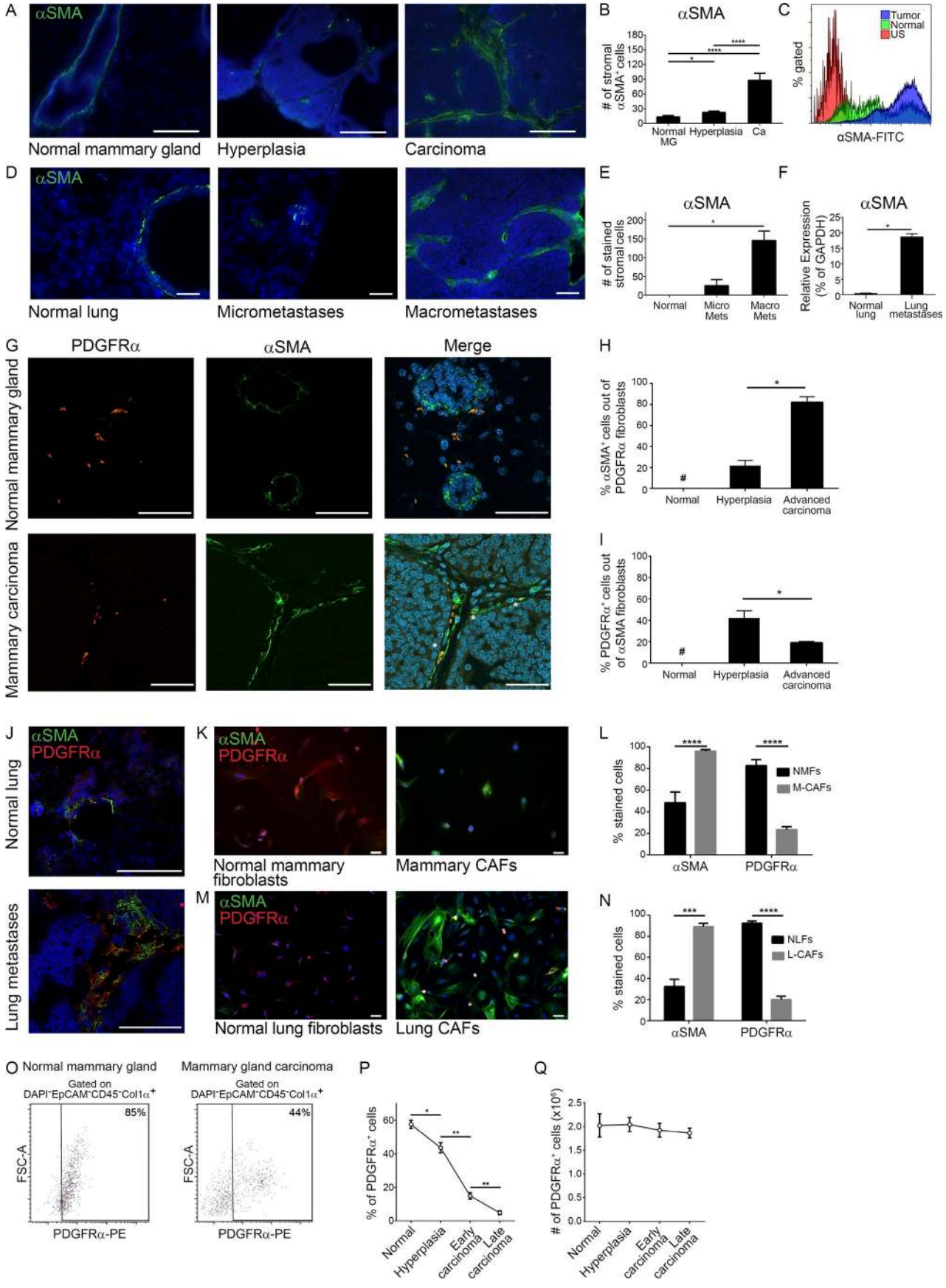

of BM smears from transplanted mice confirmed the repopulation of recipient BM with donor cells (Fig. S2 A). Immunofluorescent staining for GFP (BM derived) and αSMA (as a marker for activated fibroblasts) in mammary tissue sections from recipient mice revealed that while GFP$^+$ cells were found in both normal and tumor tissues (indicating physiological infiltration of immune cells from the BM), BM-derived activated fibroblasts (GFP$^+$αSMA$^+$ cells) were detected in mammary tumors of PyMT recipients, but not in normal mammary glands of FVB/n recipients. Moreover, analysis of metastases-bearing lungs of PyMT recipient mice revealed a subpopulation of GFP$^+$αSMA$^+$ cells in lung metastases, but not in normal lungs. Thus, BM-derived CAFs are specifically recruited to primary tumors and to lung metastatic lesions (Fig. S2, B and C).

To further analyze the subpopulation of BM-derived fibroblasts, we analyzed cell populations isolated from mammary tumors of BM transplanted mice by FACS. Interestingly, BM-derived stromal cells (GFP$^+$CD45$^-$EpCAM$^-$ cells) did not express PDGFRα, while resident stromal cells (GFP$^-$CD45$^-$EpCAM$^-$) were PDGFRα$^+$ (Fig. 2 B and Fig. S2 D). Thus, expression of PDGFRα may be specific for resident fibroblasts.

To further confirm the fibroblastic identity of the BM-derived PDGFRα$^-$ cells, the expression of various cell type–specific markers in sorted cells was analyzed by quantitative real-time PCR (qRT-PCR). Results confirmed that both GFP$^+$PDGFRα$^-$ (BM-derived) and GFP$^-$PDGFRα$^+$ (resident) cell populations expressed fibroblastic markers (Fig. 2, C and D) and did not express markers of other cell types (Fig. S2, E and F). Moreover, the same phenomenon was evident in lung metastases of BM-transplanted PyMT mice: BM-derived fibroblastic cells were recruited into lung metastases and did not express PDGFRα (Fig. 2, E–G; and Fig. S2 D). Notably, the percentages of resident CAFs and BM-derived CAFs in breast tumors were approximately equal, confirming that recruitment from the BM is a substantial source of mammary CAFs. Similarly, a distinct population of GFP$^+$PDGFRα$^-$ (BM-derived) fibroblasts was recruited to lung metastases. However, the ratio between resident and BM-derived CAFs in lung metastases could not be definitively determined since the sorted lung tissue contained the total population of lung fibroblasts and not only CAFs, as we did not sort cells from isolated lung metastases, but rather from the whole lung. Thus, the decrease in the percentage of PDGFRα$^+$ CAFs in breast tumors and lung metastases is, at least partially, a result of recruitment of a PDGFRα$^-$ fibroblastic cell population from the BM.

A major obstacle in characterizing CAFs is the lack of a single specific surface marker that can be used to detect and isolate all fibroblasts. To further verify that the BM-derived stromal cells recruited into breast tumors and lung metastases are indeed fibroblasts and to enable their unbiased isolation, we used genetically engineered mouse models which enable tracking and fate mapping of fibroblasts, expressing the fluorescent reporter genes *DsRed* or *YFP* under the *Col1α* promoter (Jiang et al., 2005). The *Col1α* promoter was shown to direct fibroblast-specific gene expression (Pallangyo et al., 2015) and thus can be used as a reliable marker of fibroblasts. Both mouse lines (*Col1α*-DsRed and *Col1α*-YFP) were backcrossed for 10 generations to the FVB/n background to be syngeneic with the MMTV-PyMT model. We crossed these mice with MMTV-PyMT mice to create PyMT;*Col1α*-DsRed/YFP double-transgenic mice, enabling unbiased isolation of heterogeneous CAF populations from primary tumors and spontaneous metastases. FACS sorting of YFP$^+$ cells from mammary tumors followed by qRT-PCR confirmed that YFP$^+$ cells express multiple fibroblast markers but do not express epithelial, endothelial, or immune cell markers. Moreover, there was almost no expression of fibroblastic markers in YFP$^-$ cells. Thus, Col1α is specific for fibroblasts and includes essentially all fibroblasts (Fig. S3, A and B).

Next, we used these double transgenic mice as donors and recipients in adoptive BM transplantations as described above for PyMT-GFP mice (Fig. 2 H). This experimental setting allows clear differentiation between host and BM-derived fibroblasts. Following irradiation, we transplanted whole BM isolated from PyMT;*Col1α*-DsRed female mice to PyMT;*Col1α*-YFP female mice. As controls, FVB/n *Col1α*-YFP mice were transplanted with BM from FVB/n *Col1α*-DsRed mice. Immunostaining of mammary tumors and lung metastases of BM-transplanted mice indicated

Figure 1. **Mammary and lung fibroblasts are activated during tumor progression. (A)** Immunofluorescence of αSMA at distinct stages of mammary carcinogenesis in the MMTV-PyMT model. *n* = 4 mice at each stage; four sections/mouse were analyzed. Bars, 100 µm. Cell nuclei, DAPI; αSMA, FITC. **(B)** Quantification of A. Results show mean ± SEM; *, P = 0.02; ****, P < 0.0001; two-tailed Mann-Whitney test. Ca, carcinoma; MG, mammary gland. **(C)** FACS analysis of αSMA in normal mammary glands and mammary tumors from FVB/n *Col1α*-DsRed or PyMT;*Col1α*-DsRed female mice, respectively. Representative of three independent experiments. US, unstained. **(D)** Immunofluorescence of αSMA in normal lungs (staining mostly around bronchi) and lungs bearing micro- or macrometastases. Representative images of multiple fields analyzed from four mice in two independent experiments. Bars, 100 µm. **(E)** Quantification of D. Results show mean ± SEM; *, P = 0.028; two-tailed Mann-Whitney test. Mets, metastases. **(F)** qRT-PCR of PDGFRα$^+$ lung CAFs, FACS sorted from a pool of end stage MMTV-PyMT mice (*n* = 5) and normal lung fibroblasts pooled from normal mice (*n* = 6). Error bars represent SD of technical repeats. *, P = 0.05; one-tailed Mann-Whitney test. **(G)** Co-staining of αSMA and PDGFRα in normal mammary gland or carcinoma. Bars, 50 µm. Asterisks mark double-labeled cells. **(H and I)** Quantification of αSMA$^+$ cells percentage within PDGFRα$^+$ stromal cells (H) and of PDGFRα$^+$ cells percentage within αSMA$^+$ stromal cells (I) in normal mammary glands and in hyperplasic or end-stage MMTV-PyMT tumors. Results show mean ± SEM. *, P = 0.028; one-tailed Mann-Whitney test. *n* = 4 mice at each stage; 4 high-power fields were analyzed for each mouse (24 high-power fields total). #, not detectable. **(J)** Co-staining of αSMA and PDGFRα in normal lungs and lung macrometastases. Bars, 100 µm. *n* = 2 mice at each stage. **(K)** Immunocytochemistry of αSMA and PDGFRα in normal mammary fibroblasts or in mammary CAFs. Bars, 50 µm. **(I)** Quantification of K. Multiple fields (at least six) from four different experiments were analyzed. Results show mean ± SEM; ****, P < 0.0001 for PDGFRα and P = 0.0002 for αSMA; two-tailed Mann-Whitney test. M-CAFs, mammary CAFs; NMFs, normal mammary fibroblasts. **(M)** Staining as in K of normal lung fibroblasts or lung CAFs. Bars, 50 µm. **(N)** Quantification of M. Multiple fields (at least seven) from three different experiments were analyzed. Results show the mean ± SEM; ***, P = 0.002; ****, P < 0.0001; two-tailed Mann-Whitney test. **(O)** FACS analysis of PDGFRα in normal mammary glands and mammary tumors pooled from three mice per group. Representative of two independent experiments. **(P and Q)** The percentage of PDGFRα$^+$ cells out of CD45$^-$ cells (P) and absolute number of these cells (Q) in normal mammary gland and mammary tumors from MMTV-PyMT mice; *n* = 5 mice in each time point. Results show mean ± SEM; *, P = 0.03; **, P = 0.0079; two-tailed Mann-Whitney test.

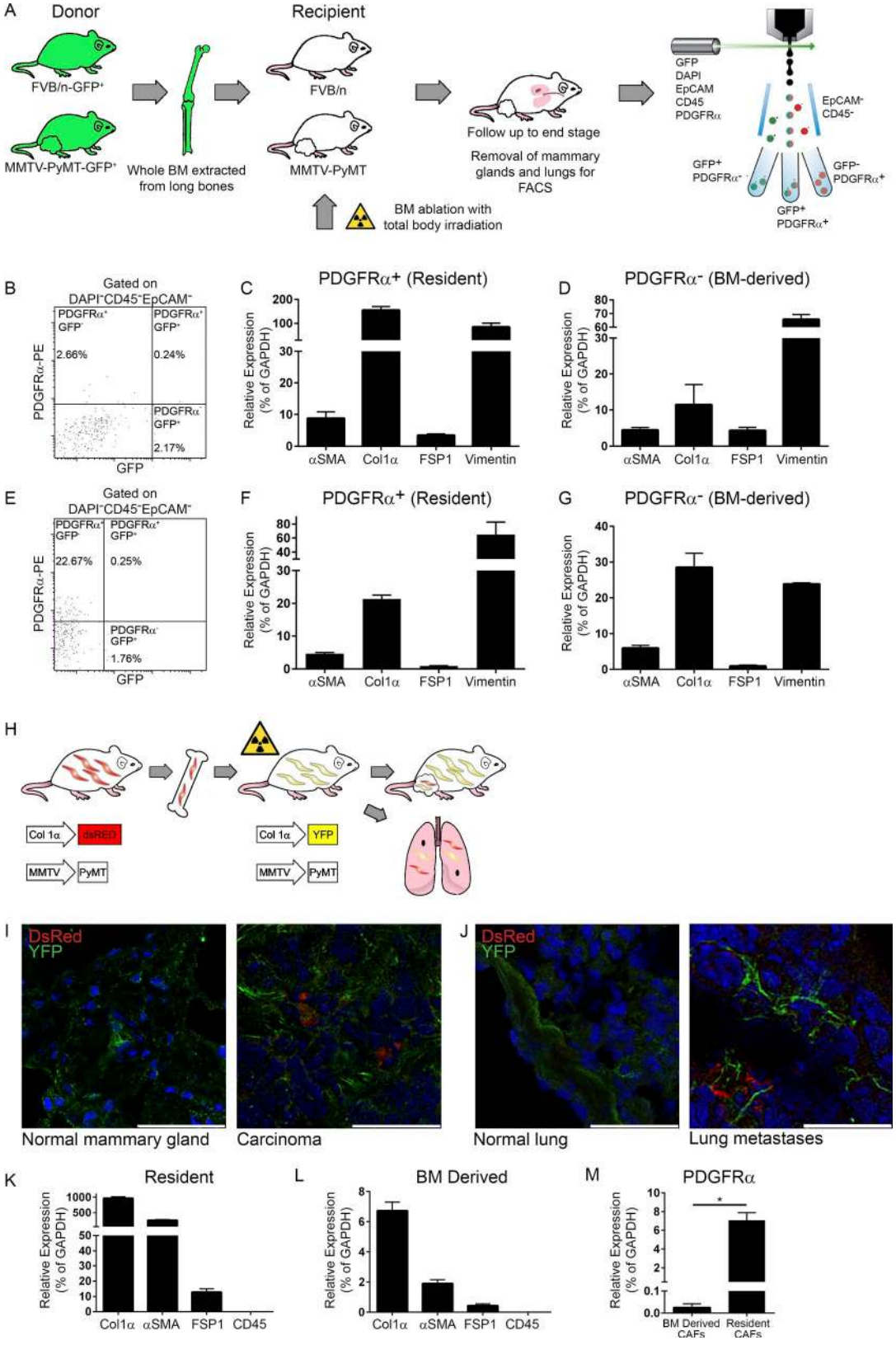

Figure 2. **A subpopulation of CAFs in mammary tumors and lung metastases are BM derived. (A)** Scheme of BM transplantation model. 6-wk-old PyMT and FVB/n female mice were transplanted with fresh whole BM isolated from age-matched GFP-PyMT and GFP female mice, respectively. Mice were sacrificed when PyMT recipients had end-stage advanced carcinoma. BM transplantation was repeated five times. **(B–G)** PDGFRα is a marker of resident fibroblasts. **(B)** FACS analysis of mammary tumors derived from a BM-transplanted PyMT mouse. $n = 4$. **(C and D)** qRT-PCR analysis of fibroblastic markers in the PDGFRα$^+$GFP$^-$ (C) and PDGFRα$^-$GFP$^+$ (D) cell populations presented in B. Results show mean ± SD of technical repeats. **(E)** FACS analysis of metastases-bearing lungs from BM-transplanted PyMT mice. $n = 2$. **(F and G)** qRT-PCR analysis of fibroblastic markers in the PDGFRα$^+$GFP$^-$ (F) and PDGFRα$^-$GFP$^+$ (G) cell populations presented

specific recruitment of BM-derived fibroblasts to tumor tissues, but not to normal glands or normal lungs (Fig. 2, I and J), suggesting that BM-derived fibroblasts are specifically recruited to tumor tissues. FACS analysis followed by qRT-PCR of characteristic cell markers confirmed that both Col1α$^+$ cell populations, DsRed$^+$ cells (BM-derived CAFs) and YFP$^+$ cells (resident CAFs), expressed markers of activated fibroblasts (Fig. 2, K and L). Moreover, only YFP$^+$ resident CAFs, but not DsRed$^+$ BM-derived CAFs, expressed PDGFRα, further validating it is a marker of resident fibroblasts (Fig. 2 M). Of note, the percentage of PDGFRα$^+$ cells within the resident fibroblasts (CD45$^-$YFP$^+$ cells) is unchanged in comparison to NMFs (Fig. S3 C). Interestingly, we found that resident CAFs expressed much higher levels of Col1α and αSMA than BM-derived CAFs, suggesting that they may have distinct functions.

BM-derived CAFs originate in MSCs

Importantly, BM-derived CAFs were CD45$^-$, implying that they are a mesenchymal-derived cell population, distinct from fibrocytes. Fibrocytes are BM-derived cells of hematopoietic origin with fibroblastic characteristics, which express hematopoietic markers (CD45 and CD34; Bucala et al., 1994). To further elucidate the cell origin of BM-derived CAFs, we isolated fresh BM cells from the tibia and femur of *Col1α*-YFP female mice and cultured them according to established methods to expand the MSC population (López-Ruano et al., 2015). Fluorescent microscopy analysis indicated that MSCs did not express Col1α, as they were YFP$^-$ (Fig. 3 A). Notably, BM-derived MSCs did not express PDGFRα (Fig. 3 B). To test whether differentiation of MSCs to CAFs can be induced by tumor cell–secreted factors, we incubated MSCs with conditioned medium (CM) from C18, a primary PyMT-derived tumor cell line established in our laboratory (Sharon et al., 2015), or from Met-1, a metastatic breast carcinoma cell line (Borowsky et al., 2005). Analysis of YFP$^+$ cells revealed that tumor cell–secreted factors, but not control medium induced the expression of Col1α in MSCs (Fig. 3, C and D). Interestingly, both the increase in cell number and in fluorescence intensity of differentiated Col1α$^+$ cells were significantly higher following incubation with C18 CM, as compared with Met-1 CM (Fig. 3, E and F). FACS analysis confirmed that differentiated BM-derived Col1α$^+$ cells did not express PDGFRα, similarly to BM-derived CAFs (Fig. 3 G). Thus, MSCs can be reprogrammed in vitro to Col1α-expressing fibroblasts by paracrine signaling from tumor cells. Importantly, the interactions between in vitro differentiated MSCs and breast tumor cells were reciprocal: MSCs that were incubated with tumor cell–secreted factors enhanced the migration of tumor cells more efficiently than activated NMFs (Fig. 3, H and I), suggesting that BM-derived CAFs may have a distinct functional role in the tumor microenvironment.

We next asked whether BM-derived MSCs differentiate in vivo to CAFs following their recruitment to tumors and whether they express Col1α in the BM or in the circulation. Analysis of YFP expression in BM or blood of PyMT;*Col1α*-YFP mice revealed that CD45$^-$Col1α$^+$ cells, which were evident in tumor tissue, were undetected in blood and in BM, suggesting that differentiation of MSCs to CAFs takes place within the tumor microenvironment. A small population of CD45$^+$Col1α$^+$ cells was found in BM, likely representing fibrocytes, which are of hematopoietic origin (Bucala et al., 1994; Fig. S3, D–F). Thus, BM-derived MSCs are specifically recruited to primary tumors and to lung metastases where they differentiate to CAFs.

Resident and BM-derived CAFs have distinct pro-inflammatory and tumor-promoting functions

To get insight on the functional distinctions between the two CAF populations in breast tumorigenesis and based on our previous findings that CAFs mediate tumor-promoting inflammation (Erez et al., 2010; Sharon et al., 2015), we analyzed the immune-related transcriptome of CAFs from different origins. To that end, we extracted total RNA from sorted populations of BM-derived or resident CAFs that were isolated from mammary tumors or from lungs bearing metastases in BM-transplanted mice and analyzed the expression of 561 immune-related genes using the NanoString nCounter gene expression panel. Analysis of the panel results revealed unique gene expression of resident versus BM-derived CAFs (Fig. 4 A). Interestingly, analysis of the results by Venn diagrams as well as hierarchical clustering indicated tissue-specific imprinting on gene expression: BM-derived CAFs recruited to mammary tumors or to lung metastasis were more similar to resident CAFs of breast and lungs, respectively, than to other BM-derived CAFs (Fig. 4, B and C), suggesting that reprogramming of immune-related functions mediated by BM-recruited CAFs is affected by the organ milieu to which they were recruited, more than by their origin.

Notably, among the genes that were most differentially up-regulated in resident CAFs in both mammary tumors and in lung metastases, were genes related to extracellular matrix remodeling and recruitment of BM-derived cells (e.g., fibronectin, TGFβR2, and SDF-1), consistent with our observation that Col1α was more highly expressed in resident CAFs than in BM-derived

in E. Error bars represent SD of technical repeats. **(H–M)** A subpopulation of Col1α$^+$ CAFs in mammary tumors and lung metastases are BM derived. **(H)** Scheme of BM transplantation model. Following BM ablation with total body irradiation, 6-wk-old PyMT;*Col1α*-YFP or FVB/n *Col1α*-YFP female mice were transplanted with fresh whole BM isolated from age-matched PyMT;*Col1α*-DsRed or FVB/n *Col1α*-DsRed female mice, respectively. Mice were analyzed when PyMT;*Col1α*-YFP recipients had advanced carcinoma tumors. BM transplantations were repeated five times (n = 2–4 mice in each cohort). **(I)** Immunofluorescent staining of resident (YFP) and BM-derived (DsRed) cells in normal mammary glands from FVB/n *Col1α*-YFP recipients or in mammary tumors from PyMT;*Col1α*-YFP recipient mice. Bars: 50 µm (left); 25 µm (right). **(J)** Immunofluorescent staining as in I in normal lungs from FVB/n *Col1α*-YFP recipients or in lung macrometastases from PyMT;*Col1α*-YFP recipients. Bars: 50 µm (left); 25 µm (right). For I and J, multiple fields from at least three mice were analyzed. Cell nuclei, DAPI; YFP, Alexa Fluor 488; DsRed, Rhodamine. **(K)** qRT-PCR analysis of fibroblastic and leukocyte markers in the YFP$^+$ (resident) cells, FACS sorted from mammary tumors in the PyMT;*Col1α*-YFP recipient mice (n = 2, pooled). Error bars represent SD of technical repeats. **(L)** qRT-PCR analysis as above in the DsRed$^+$ (BM-derived) cells isolated from recipient mice (n = 2, pooled). Error bars represent SD of technical repeats. **(M)** qRT-PCR analysis of PDGFRα expression in YFP$^+$ (resident) and DsRed$^+$ (BM-derived) cells isolated from recipient mice (pooled). Error bars represent SD of technical repeats. *, P = 0.05; one-tailed Mann-Whitney test.

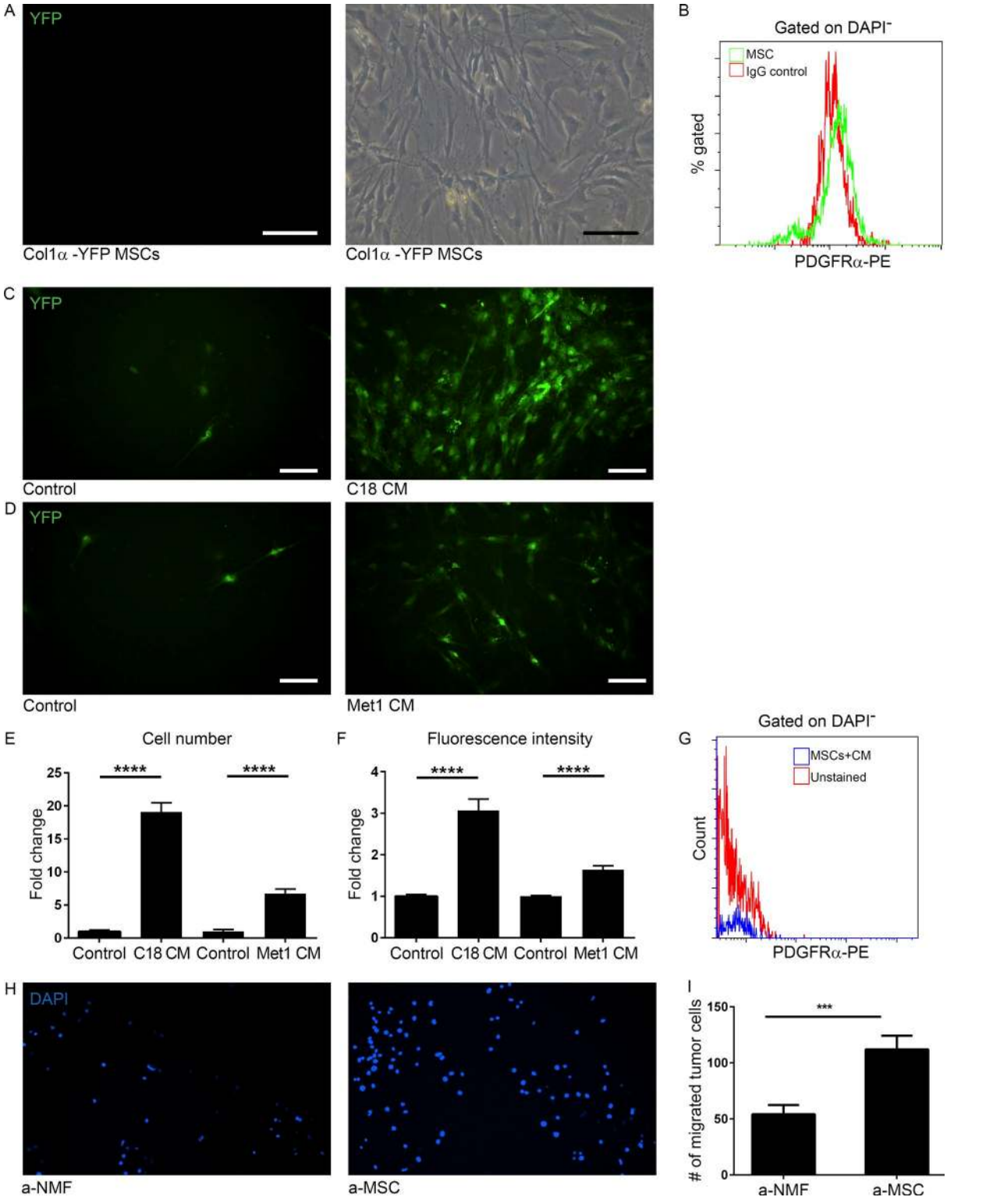

Figure 3. **Tumor cell–secreted factors induce differentiation of BM-derived mesenchymal stem cells to CAFs. (A)** Images of cultured mesenchymal stem and progenitor cells (MSCs) produced from total BM of FVB/n *Col1a*-YFP mice. Light microscopy (right panel) and green fluorescence (left panel). $n = 4$. Representative of two independent experiments. Bars, 100 µm. **(B)** FACS analysis of PDGFRα in MSCs. **(C and D)** Fluorescent microscope images of MSCs that were incubated with C18 CM (C, right) or Met-1 CM (D, right) for 3 wk and compared with controls cultured in 10% FCS medium (left panels). YFP⁺ cells are shown in green. $n = 4$. Bars, 100 µm. **(E and F)** Quantification of YFP⁺ cell number (E) and fluorescence intensity (F) of images presented in C and D. 30 fields of CM and 10 fields of control were analyzed. Error bars represent SEM. ****, $P < 0.0001$, two-tailed Mann-Whitney test. **(G)** FACS analysis of PDGFRα in MSCs incubated with Met-1 CM. **(H)** Migration transwell assay of Met-1 mammary tumor cells incubated with tumor-activated NMFs (a-NMFs) or MSCs (a-MSCs) for 24 h. Representative images of 24 fields analyzed from duplicate wells. **(I)** Quantification of data shown in H. Results show mean ± SEM. ***, $P = 0.0008$; two-tailed Mann-Whitney test.

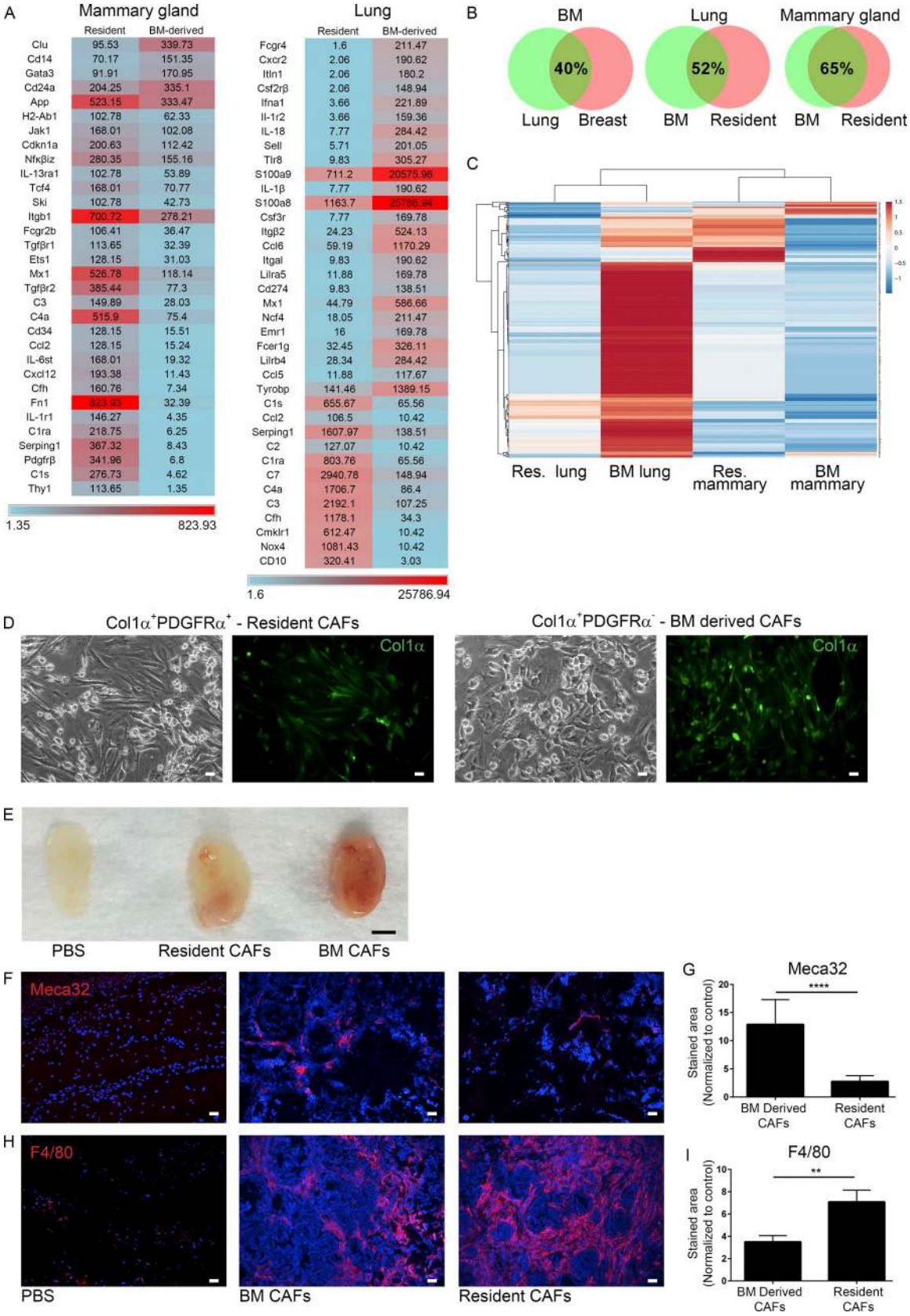

Figure 4. **Resident and BM-derived CAFs express distinct immune-related genes.** Following BM transplantation, resident and BM-derived CAFs from mammary tumors and lungs bearing macrometastases of recipient mice were tested for the expression of 561 immunology-related genes using the NanoString nCounter gene expression panel. *n* = 2 mice in each group. **(A)** Heat map presentation of differentially expressed genes of resident versus BM-derived CAFs in primary tumors (left) and lungs bearing macrometastases (right). **(B)** Venn diagrams of the 40 most highly expressed genes in each cell population. **(C)**

CAFs (Fig. 2). Pro-inflammatory genes were up-regulated in all four fibroblast cell populations in a tissue-specific manner.

Hallmark functions of CAFs in facilitating tumorigenesis include pro-angiogenic signaling and immune cell recruitment to the tumor microenvironment (Gascard and Tlsty, 2016; Kalluri, 2016; Cohen et al., 2017). Therefore, to further investigate the tumor-promoting functions of resident and BM-derived CAFs in vivo, we analyzed their ability to induce angiogenesis and to enhance macrophage recruitment. To that end, we isolated resident CAFs (EpCAM$^-$CD45$^-$Col1α$^+$PDGFRα$^+$) and BM-derived CAFs (EpCAM$^-$CD45$^-$Col1α$^+$PDGFRα$^-$) from mammary tumors of PyMT;*Col1α*-YFP$^+$ female mice (Fig. 4 D) and injected them in a Matrigel plug to FVB/n female mice. Plugs were extracted 3 wk after injection and analyzed by immunostaining for blood vessel density (Meca32) and macrophage recruitment (F4/80). Strikingly, we found significant differences between resident and BM-derived CAFs: BM-derived CAFs were more efficient in inducing angiogenesis, which was evident even by macroscopic examination (Fig. 4 E). Quantitative immunofluorescent analysis of plug sections confirmed that blood vessels were more abundant and also markedly larger in diameter in the plugs injected with BM-derived CAFs (Fig. 4, F and G; and Fig. S4, A and B). However, resident CAFs recruited significantly more macrophages than BM-derived CAFs (Fig. 4, H and I).

We next set out to investigate the distinct functional role of BM-derived CAFs in mammary tumor growth in vivo. To that end, we isolated repopulating hematopoietic stem cells (HSCs; c-Kit$^+$Lin$^-$Sca-1$^+$CD34$^-$CD45$^+$) and MSCs (c-Kit$^+$Lin$^-$Sca-1$^+$CD34$^-$CD45$^-$) from BM of *Col1α*-DsRed female mice and used them for adoptive BM transplantations into irradiated *Col1α*-YFP recipient mice. Recipient mice were transplanted with either HSCs only or with HSCs and MSCs. 2 wk following transplantation, mice were orthotopically injected with Met-1 cells (Fig. 5 A and Fig. S4 C). Importantly, we confirmed the presence of BM-derived CAFs in the injected tumors by analyzing DsRed expression. DsRed expression was significantly higher in tumors from mice transplanted with MSCs, as compared with mice transplanted with HSCs only, indicating the recruitment of BM-derived fibroblasts of mesenchymal origin in these mice (Fig. 5 B). The low level of DsRed expression in mice injected with HSCs only may reflect the presence of Col1α-expressing fibrocytes of hematopoietic origin. Analysis of tumor growth and tumor volumes revealed that tumors in mice that were transplanted with HSCs and MSCs grew faster and were significantly larger than tumors in mice transplanted with HSCs only (Fig. 5, C and D). Moreover, analysis of apoptosis indicated that tumors in mice injected with HSCs and MSCs had significantly less apoptotic cells, quantified by cleaved caspase-3 and expression of Annexin V (Fig. 5, E–G; and Fig. S4 D). Thus, recruitment of BM-derived CAFs facilitates tumor growth and viability of tumor cells in vivo. To further elucidate the functional role of BM-derived CAFs in facilitating tumor growth, we analyzed the presence of macrophages and blood vessel density in tumors of transplanted mice. In agreement with the plug assay results, macrophage recruitment was not significantly affected by the presence of BM-derived CAFs, as resident CAFs are functional in both transplanted groups (HSCs only as well as HSCs and MSCs; Fig. 5, H and I). Furthermore, analysis of blood vessel density (Meca32 staining) indicated that tumors that contained both resident and BM-derived CAFs were significantly more vascularized than tumors with resident CAFs only (Fig. 5, J and K). Thus, recruitment of BM-derived CAFs is functionally important for promoting tumor growth and viability of cells, most likely via enhancement of angiogenesis.

To get mechanistic insight on the pro-angiogenic activity of BM-derived CAFs, we revisited the gene expression data obtained by the NanoString analysis. The most up-regulated gene in BM-derived mammary CAFs was Clusterin.

Clusterin is a multifunctional stress-associated glycoprotein with anti-apoptotic functions, shown to be overexpressed in various cancers including breast carcinomas (Koltai, 2014; Tellez et al., 2016). Clusterin is up-regulated in tumors in response to therapy and was shown to contribute to chemoresistance (Koltai, 2014). Moreover, Clusterin was implicated in angiogenesis in ovarian cancer (Fu et al., 2013). Encouraged by these findings we set out to elucidate the role of Clusterin in the pro-angiogenic function of BM-derived CAFs. Analysis of Clusterin expression in resident versus BM-derived CAFs isolated from tumors of PyMT;*Col1α*-YFP mice confirmed that Clusterin is up-regulated in BM-derived CAFs (Fig. 6 A). To assess the effect of Clusterin inhibition on the pro-angiogenic activity of BM-derived CAFs, we knocked down its expression in BM-derived CAFs isolated from mammary tumors of PyMT;*Col1α*-YFP mice by siRNA transduction, using a modified mixture of four targeting siRNAs that provide an extended duration of gene knockdown (Fig. 6 B). Notably, while CM of BM-derived CAFs had a modest but significant growth-promoting effect on endothelial cells, knockdown of Clusterin resulted in a significant reduction in the growth of endothelial cells in vitro (Fig. 6 C), suggesting that Clusterin secreted by BM-derived CAFs facilitates endothelial cell proliferation. To assess the effect of Clusterin inhibition on angiogenesis in vivo, we next performed a plug assay. Resident CAFs (EpCAM$^-$CD45$^-$Col1α$^+$PDGFRα$^+$) and BM-derived CAFs (EpCAM$^-$CD45$^-$Col1α$^+$PDGFRα$^-$) were isolated from mammary tumors of PyMT;*Col1α*-YFP female mice, cultured, and transduced with siClusterin or siControl for 48 h, after which they were injected to recipient mice (Fig. 6 D). Strikingly, macroscopic analysis of

Hierarchical clustering of total expressed genes in resident and BM-derived CAFs from primary tumors and lungs bearing macrometastases. Scaling method: unit variance scaling; PCA method: single-value decomposition with imputation. **(D–I)** PDGFRα$^+$-resident CAFs and PDGFRα$^-$ BM-derived CAFs have distinct tumor-promoting functions. Resident CAFs (EpCAM$^-$CD45$^-$Col1α$^+$PDGFRα$^+$) and BM-derived CAFs (EpCAM$^-$CD45$^-$Col1α$^+$PDGFRα$^-$) were isolated from mammary tumors of PyMT;*Col1α*-YFP female mice, cultured, and injected in a Matrigel plug to FVB/n female mice. $n = 4$. Experiments were repeated twice. **(D)** Light and fluorescent microscopy of resident CAFs (left) and BM-derived CAFs (right) cultures preinjection. Bars, 30 µm. **(E)** Representative images of the plugs extracted 3 wk after injection. Bar, 5 mm. **(F and H)** Immunostaining of Meca32 (F) or F4/80 (H). 5 sections per plug were stained and 5 fields per section were analyzed for a total of 100 fields per cell type. Bars, 30 µm. **(G and I)** Quantification of staining presented in F and H performed with ImageJ software. Results are normalized to control (PBS-only plugs). Error bars represent SEM. ****, $P < 0.0001$ (G); **, $P = 0.0041$ (I); two-tailed Mann-Whitney test.

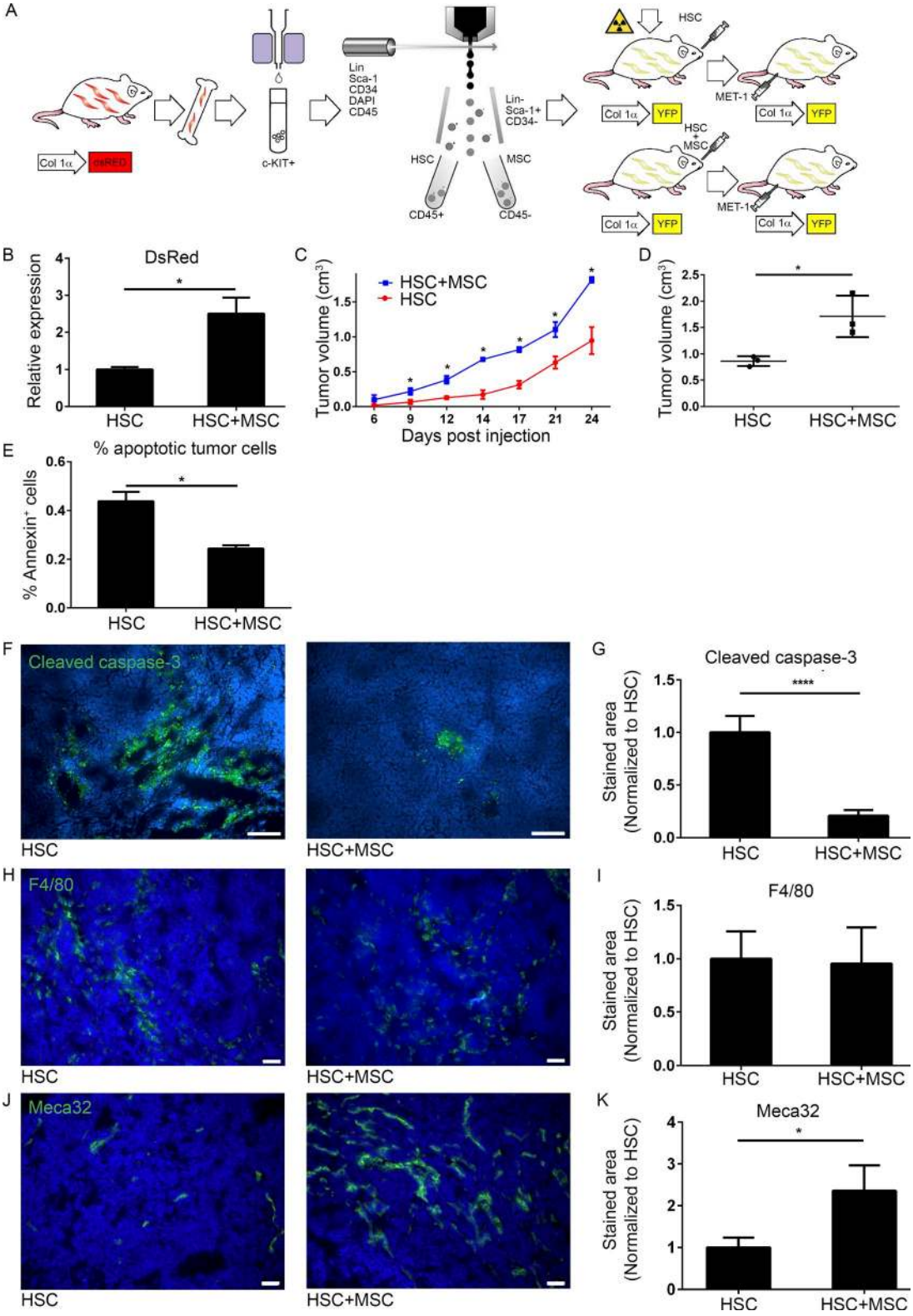

Figure 5. **BM-derived CAFs are functionally important for tumor growth. (A)** Scheme of transplantation model. Following BM ablation with total body irradiation, 6-wk-old FVB/n Col1α-YFP female mice were transplanted with either HSCs only or HSCs and MSCs isolated and sorted from age-matched FVB/n *Col1α*-DsRed female mice. 2 wk following transplantation, Met-1 cells were injected into the right inguinal mammary gland of the transplanted mice. Mice were euthanized 24 d after injection and tumors were analyzed. Experiment was repeated twice, $n \geq 3$ mice per group for each experiment. **(B)** qRT-PCR analysis of DsRed expression in FVB/n *Col1α*-YFP recipient mice of both experiments, transplanted as indicated. Results were normalized to mGUS and to control (HSC-only transplantation). Error bars represent SEM. *, P = 0.003, two-tailed Mann-Whitney test. **(C)** Growth curve of tumors describes in A. $n = 3$ mice per group. Error bars represent SEM. *, P = 0.05; one-tailed Mann-Whitney test. **(D)** Tumor volumes of injected tumors at end-point. *, P = 0.05; one-tailed Mann-Whitney test. **(E)** FACS analysis of Annexin V in tumors from HSCs only or HSC and MSC–transplanted mice. Percentage from total nonleukocyte ($CD45^-$) epithelial

the plugs indicated that plugs injected with BM-derived CAFs in which Clusterin was knocked down were less vascularized than control plugs (Fig. 6 E). Analysis of blood vessel density in tissue sections revealed that knockdown of Clusterin significantly inhibited angiogenesis induced by BM-derived CAFs, implicating Clusterin as an important mediator of their pro-angiogenic and tumor-promoting function (Fig. 6, F and G).

Thus, BM-derived CAFs have distinct gene expression and tumor-promoting functions, and their enhancement of tumor growth is mediated, at least in part, by up-regulation of the pro-angiogenic factor Clusterin.

Decreased PDGFRα in human tumors correlates with worse outcome

Finally, we asked whether the decrease in PDGFRα$^+$ CAFs during tumor progression is operative also in human cancer. To that end, we analyzed a cohort of 728 breast cancer patients from The Cancer Genome Atlas (TCGA) database. Analysis of the expression data in human breast cancer revealed a significant decrease in the expression of PDGFRα (Fig. 7 A). Moreover, this down-regulation of PDGFRα was evident in multiple other human tumors suggesting that it may be a general phenomenon in cancer (Fig. 7 B and Fig. S5 E). Notably, lower levels of PDGFRα were associated with worse outcome in several subtypes of human breast cancer (Fig. 7 C and Fig. S5, A–D). The expression data in the TCGA dataset is of total tumors, and PDGFRα is expressed in both tumor cells and stromal cells in some carcinomas (Carvalho et al., 2005). Nevertheless, the significant reduction we observed in the expression of PDGFRα in human tumors may be related to the influx of BM-derived PDGFRα$^-$ stromal cells.

To assess whether the decreased expression of PDGFRα in human breast tumors was associated with recruitment of PDGFRα$^-$ CAFs, we analyzed tissue sections from breast cancer patients or normal breast retrieved from the Human Protein Atlas (Uhlén et al., 2015). Analysis of the staining revealed that only part of the CAFs in breast tumors were PDGFRα$^+$, and a distinct population of PDGFRα$^-$ CAFs was evident in tumors. Conversely, in normal breast, the vast majority of fibroblasts were PDGFRα$^+$, similar to our observations in mice (Fig. 7, D–F). Collectively, these findings suggest that the decrease in PDGFRα in human breast tumors is at least partially a result of the recruitment of PDGFRα$^-$ BM-derived CAFs, which may affect disease progression and outcome.

Discussion

In this study, we described a novel subpopulation of CAFs that originate in the BM and are recruited to the microenvironment niche of both primary tumors and lung metastases in breast cancer. Upon recruitment, they acquire specific functional CAF characteristics including the ability to attract immune cells and induce angiogenesis. Data from human patients suggest that this unique BM-derived CAF population may have a deleterious effect on survival.

BM-derived mesenchymal cells were previously suggested to contribute to the stromal compartment of tumors (Direkze et al., 2004; Anderberg and Pietras, 2009; Öhlund et al., 2014; Barcellos-de-Souza et al., 2016), but their in vivo differentiation to CAFs and characterization of their distinct functional role in tumors is largely unknown. Moreover, the origin of CAFs in lung metastases was not previously demonstrated. We show that BM-derived MSCs are specifically recruited to mammary tumors and to lung metastases and constitute a substantial fraction of CAFs in the tumor microenvironment, in addition to resident CAFs. Our findings demonstrate that recruited BM-derived mesenchymal cells differentiate in the tumor tissue to Col1α-expressing CAFs that, unlike resident CAFs, do not express PDGFRα. Furthermore, BM-derived CAFs are reprogrammed in the tissue to express pro-inflammatory genes that are specific to the tissue to which they were recruited. Functionally, we demonstrated that BM-derived CAFs are important for promoting tumor growth in vivo. Moreover, resident CAFs and BM-derived CAFs were distinct in their ability to induce angiogenesis and to recruit macrophages.

CAFs are a heterogeneous cell population, with multiple origins including resident fibroblasts, adipocytes, and BM-derived precursors (Orimo and Weinberg, 2007). The role of MSCs in modulating tumor growth has been controversial (Mishra et al., 2009; Bergfeld and DeClerck, 2010), partially as a result of their unclear definition. MSCs were shown to be recruited to inflammation-induced gastric cancer (Quante et al., 2011) and to facilitate breast cancer metastasis when co-injected with a tumor cell line (Karnoub et al., 2007; Yu et al., 2017). However, the in vivo differentiation of MSCs to CAFs was not previously shown. By generating transgenic mouse models of breast carcinogenesis and spontaneous lung metastasis in which all fibroblasts are genetically labeled, we were able to track and demonstrate the recruitment of BM-derived cells to mammary tumors and to lung metastases. We further validated the mesenchymal origin of BM-derived CAFs by performing BM transplantations of labeled BM hematopoietic or mesenchymal progenitor cells (HSCs and MSCs). Moreover, we show that MSCs can differentiate to Col1α-expressing CAFs as a result of paracrine signaling from tumor cells, in agreement with previous studies (Mishra et al., 2008). Notably, our in vivo findings indicate that differentiation of MSCs to CAFs occurs in the tumor tissue to which they were recruited: MSCs in the BM or in the circulation did not express Col1α, which was induced once they had reached mammary tumors or lung metastases. Interestingly, a previous

(EpCAM$^+$) cells. *n* = 3 mice per group. Error bars represent SEM. *, P = 0.05; one-tailed Mann-Whitney test. **(F)** Immunofluorescence of cleaved caspase-3 in tumor sections from transplanted mice. Bars, 50 µm. **(G)** Quantification of staining presented in F performed with ImageScope software and Aperio Positive Pixel Count Algorithm. 2 whole sections per mouse were analyzed for a total of 12 whole sections per group. Results are normalized to control (HSC-only transplantation). Error bars represent SEM. ****, P < 0.0001, two-tail Mann-Whitney test. **(H and J)** Immunofluorescence of F4/80 (H) or Meca32 (J) in tumor sections from transplanted mice. Multiple fields were analyzed from each tumor for a total of 40 fields per group per stain. Bars, 50 µm. **(I and K)** Quantification of staining presented in H and J performed with ImageJ software. Results are normalized to control (HSC-only transplantation). Error bars represent SEM. P = 0.86 (I); *, P = 0.01 (K); two-tailed Mann-Whitney test.

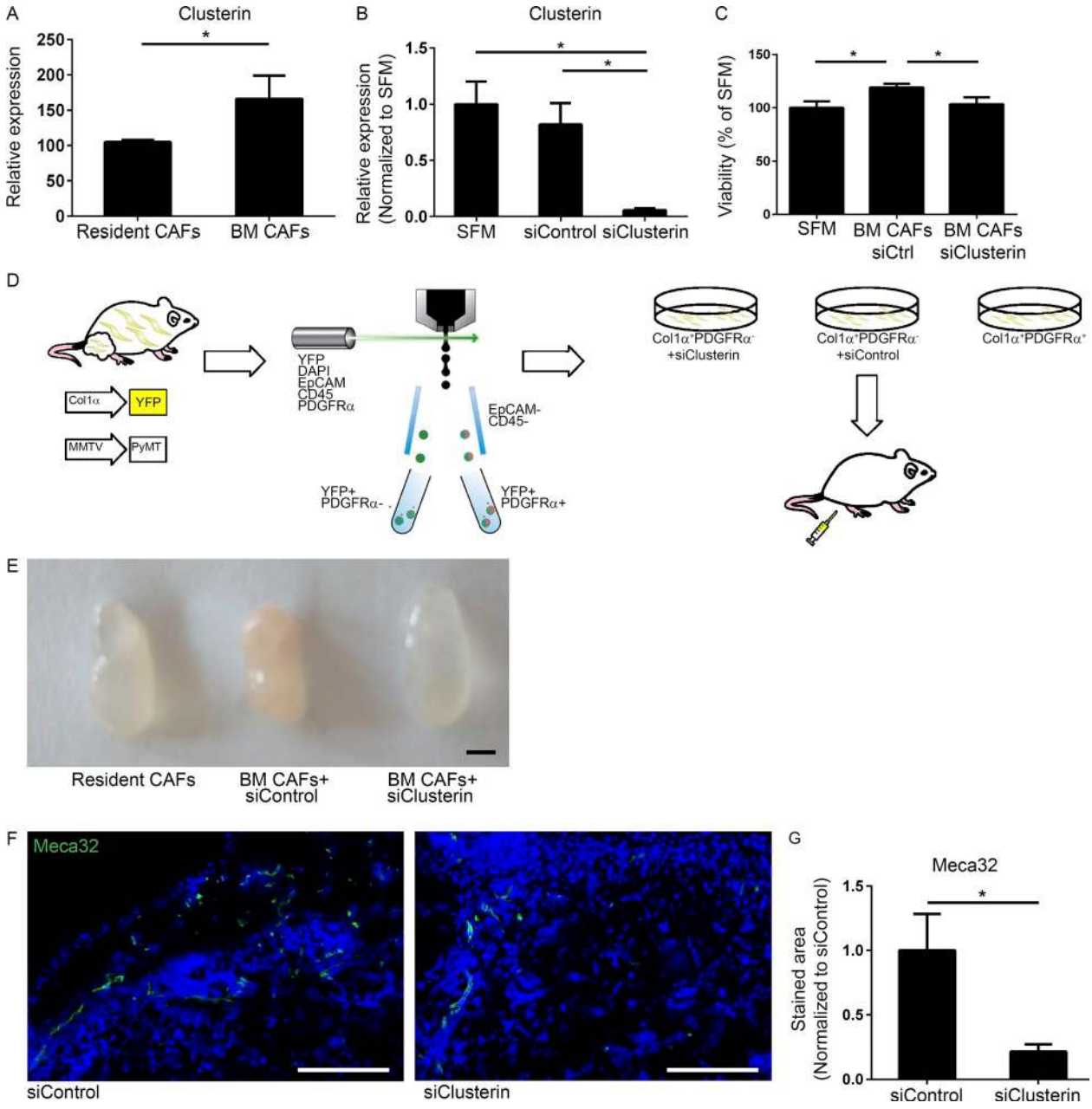

Figure 6. **BM-derived CAFs enhance angiogenesis via Clusterin. (A)** qRT-PCR analysis of Clusterin expression in resident ($CD45^-Col1\alpha^+PDGFR\alpha^+$) and BM-derived ($CD45^-Col1\alpha^+PDGFR\alpha^-$) CAFs, FACS sorted from tumors of PyMT;*Col1a*-YFP mice. Results were normalized to mGUS. Error bars represent SD of technical repeats. *n* = 3 mice; *, P = 0.05; one-tailed Mann-Whitney test. **(B)** qRT-PCR analysis of Clusterin expression in BM-derived ($CD45^-Col1\alpha^+PDGFR\alpha^-$) CAFs, FACS sorted from tumors of PyMT;*Col1a*-YFP mouse and cultured with SFM, siClusterin, or siControl. Results were normalized to GAPDH and to control. SFM, serum-free medium. Error bars represent SD of technical repeats. *, P = 0.05; one-tailed Mann-Whitney test. **(C)** Methylene blue viability assay of endothelial cells incubated with CM of BM-derived CAFs treated with siClusterin or siControl. Data presented as percent of SFM. *n* = 2 wells per cell type. Error bars represent SD of technical repeats. *, P = 0.0325; one-tailed Mann-Whitney test. **(D)** Scheme of Matrigel plug experiment. Resident CAFs ($EpCAM^-CD45^-Col1\alpha^+PDGFR\alpha^+$) and BM-derived CAFs ($EpCAM^-CD45^-Col1\alpha^+PDGFR\alpha^-$) were isolated from mammary tumors of PyMT;*Col1a*-YFP female mice, cultured and treated with siClusterin or siControl for 48 h, after which they were injected in a Matrigel plug with additional siRNA to 6–8-wk-old FVB/n female mice. *n* = 2 mice in the control group and 6 mice in the siClusterin group. **(E)** Representative images of plugs that were extracted 1 wk after injection. Bar, 5 mm. **(F)** Immunostaining of Meca32 in Matrigel plugs as in E. Representative images (control group: *n* = 20 sections; siClusterin group: *n* = 12 sections). Bar, 50 µm. **(G)** Quantification of F performed with ImageScope software and Aperio Positive Pixel Count Algorithm. Error bars represent SEM. *, P = 0.02, two-tailed Mann-Whitney test.

study of inflammation-induced gastric cancer suggested that tumor-derived paracrine signaling contributes to modification of the MSC niche within the BM (Quante et al., 2011). Thus, tumor-specific mechanisms of recruitment could be operative in different tumor types. Our results suggest that while expansion of the MSC niche in the BM may be induced systemically, differentiation to pro-inflammatory CAFs only occurs at the tumor site. Once recruited, MSCs differentiate to a functionally distinct population of pro-angiogenic and pro-inflammatory CAFs that can be distinguished from resident CAFs by their lack of expres-

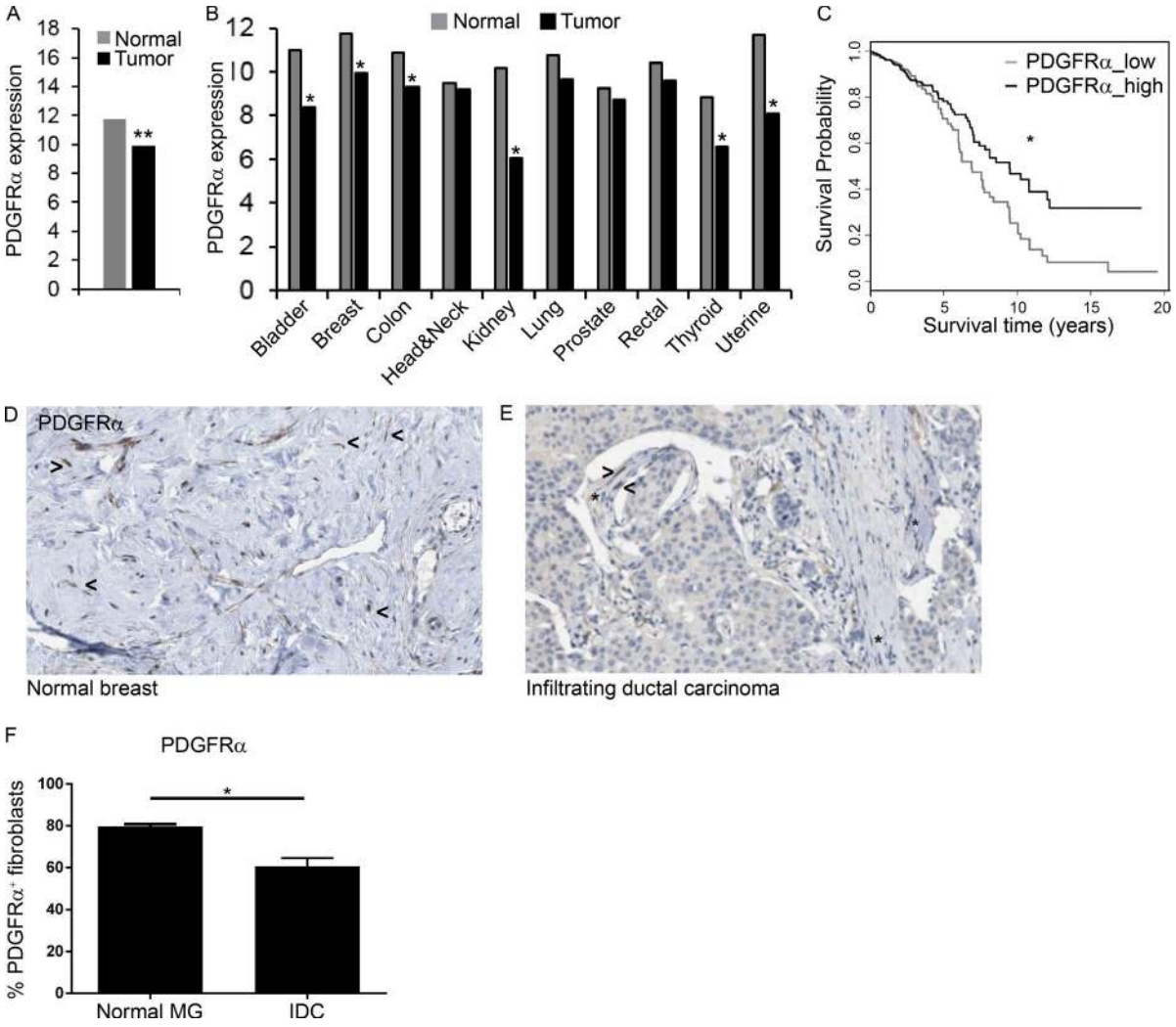

Figure 7. **Decreased PDGFRα in human tumors correlates with worse prognosis.** Gene expression datasets in 10 diverse cancer types from TCGA and the newer TCGA PANCAN database were analyzed. **(A)** PDGFRα $\log_2$ fragments per kilobase of transcript per million mapped reads expression values in breast cancer patients (n = 649) compared with normal breast tissue (n = 79). **, P < 0.001, Student's t test, and fold-change >1.5. **(B)** Expression levels of PDGFRα across 10 diverse types of normal and malignant tissues (see Fig. S5 E for details of cohorts). **, P < 0.001, Student's t test, and fold-change >1.5. **(C)** Kaplan–Meier plot for overall survival rates at high and low expression levels of PDGFRα compared with the median expression (black and gray curves, respectively). Pre-processed and normalized RNA-seq gene expression data from the new TCGA were analyzed (n = 1,215). *, P < 0.05; χ^2 test. **(D and E)** IHC of PDGFRα in tissue sections from human normal breast (n = 2; D) and invasive ductal carcinoma (n = 12; E) retrieved from the Human Protein Atlas. Asterisks, PDGFRα$^+$ fibroblasts; arrowheads, PDGFRα$^-$ fibroblasts. **(F)** Quantification of D and E. Error bars represent SEM. **, P = 0.022; two-tailed Mann-Whitney test. IDC, intraductal carcinoma; MG, mammary gland.

sion of PDGFRα. Since the reciprocal interactions in the tumor microenvironment are affected by multiple cell types, it is conceivable that the recruitment of MSCs to tumors as well as their differentiation to CAFs may also be affected by other cell types in the microenvironment including immune cells, endothelial cells, and resident fibroblasts.

Interestingly, BM-derived stromal cells were shown to home preferably to sites of tissue injury, and give rise to myofibroblasts (Direkze et al., 2003) and to Col1-producing cells in the dermis of cutaneous wounds (Fathke et al., 2004). Moreover, recruitment from the BM was demonstrated to be a significant source for functional myofibroblasts in kidney fibrosis (Broekema et al., 2007; LeBleu et al., 2013). Our findings suggest that these physiological mechanisms are hijacked by tumors, resulting in an influx of MSCs to breast tumors and lung metastases. The relative contribution of BM-derived fibroblasts to the overall population of CAFs may be tumor type-specific (Arina et al., 2016).

PDGFRα was shown to be robustly expressed by fibroblasts (Erez et al., 2010; Driskell et al., 2013). Its ligands, PDGF-AA and PDGF-CC, are often highly expressed in various carcinomas (Pietras et al., 2008; Cao, 2013) and have been shown to stimulate proliferation of CAFs and to regulate the reactive stromal phenotype and desmoplastic reaction in tumors (Shao et al., 2000; Pietras et al., 2008; Öhlund et al., 2014), as well as the tumor-promoting effects of CAFs (Östman, 2017). We found that BM-derived CAFs do not express PDGFRα, suggesting that other pathways are operative in the signaling between tumor cells and this CAF population. Interestingly, a population of PDGFRα$^-$ CAFs was previously reported in a model of transplantable melanoma, but their origin was not studied (Anderberg et al., 2009).

While transgenic mouse models of breast cancer have limitations and may not authentically mimic the etiology and clinical course of human breast cancer, analysis of clinical data revealed a decrease in PDGFRα expression in human breast cancer patients, suggesting that recruitment of PDGFRα$^-$ CAFs from the BM is operative also in human disease. Moreover, we found that lower expression of PDGFRα in estrogen receptor (ER)$^+$ and progesterone receptor (PR)$^+$ breast cancer patients was associated with reduced survival, suggesting that PDGFRα$^-$ BM-derived CAFs may impact worse clinical outcome.

Therapeutic targeting of CAFs remains a challenge as a result of incomplete knowledge of their origin and functional contribution. Our findings of two functionally distinct CAF populations that can be differentiated by their expression of PDGFRα elucidate some of the complexity associated with functional characterization of CAFs and may contribute to patient stratification and to specific targeting of CAFs in breast cancer.

Analysis of gene expression in resident and BM-derived CAFs from mammary tumors or lung metastases revealed transcriptional changes that were distinct and tissue specific, implicating organ-specific microenvironments in reprogramming of stromal cells. Moreover, BM-derived CAFs were functionally important for tumor growth and were more efficient than resident CAFs in promoting angiogenesis. Thus, MSCs are specifically recruited to neoplastic tissues, where they are reprogrammed in a tissue-specific manner to mediate tumor-promoting inflammation and facilitate angiogenesis and tumor growth.

We demonstrated that the molecular mechanism by which BM-derived CAFs promote angiogenesis is mediated by up-regulation of the secreted glycoprotein Clusterin, shown to affect tumor cell growth, angiogenesis, and resistance to therapy (Fu et al., 2013; Koltai, 2014; Tellez et al., 2016; Wang et al., 2018). Moreover, Clusterin was found to be up-regulated in human breast cancer, in correlation with tumor progression (Redondo et al., 2000; Yom et al., 2009). However, in these studies the expression of Clusterin was analyzed in total tumor tissue sections, without specifically analyzing the expression in CAFs. Our results implicate Clusterin in a subpopulation of CAFs and suggest that its expression by BM-derived CAFs contributes to its pro-tumorigenic role: knockdown of the expression of Clusterin in BM-derived CAFs attenuated their pro-angiogenic activity in vivo. Importantly, targeting of Clusterin by an antisense oligodeoxynucleotide (OGX-011; Custirsen) was shown to be effective in combination with other drugs using multiple human tumor cell lines (Kususda et al., 2012; Tang et al., 2012; Lamoureux et al., 2014). OGX-11 was also tested in clinical trials in metastatic prostate cancer (Beer et al., 2017), and other trials are ongoing. However, the suggested mechanism of action for Clusterin inhibition in these studies is tumor cell–intrinsic, via the anti-apoptotic activity of Clusterin. Our findings suggest that the potential benefit of targeting Clusterin is also via its role in the tumor microenvironment, due to its CAF-mediated functions, which enhance tumor angiogenesis and growth.

In summary, our comprehensive characterization of BM-recruited CAFs in breast cancer and lung metastases shows that the expression of PDGFRα distinguishes between two distinct CAF populations in the microenvironment of breast tumors. The identification of PDGFRα as a differential marker for these two CAF populations provides new insight into the contribution of BM-derived mesenchymal cells to the formation of a pro-inflammatory, tumor-promoting microenvironment. Better characterization of the specific functional roles of CAF populations in the tumor microenvironment can form the mechanistic basis for the development of novel therapeutic manipulations and cotargeting of BM-derived CAFs as adjuvant anti-cancer therapies.

Materials and methods

Mice and human samples

All experiments involving animals were approved by the Tel Aviv University Institutional Animal Care and Use Committee. All experiments were performed using 6–8-wk-old female mice, unless otherwise stated. FVB/n mice were purchased from Harlan. FVB/N-Tg (MMTV-PyMT)634Mul/J mice and FVB.Cg-Tg(CAG-EGFP)B5Nagy/J were purchased from The Jackson Laboratory. FVB/n Col1α-DsRed/YFP mice were a gift from G. Leone and M. Ostrowski (The Ohio State University, Columbus, OH). All animals were maintained within the Tel Aviv University specific pathogen–free facility.

Immunostaining

Mouse samples tissue preparation

Mammary glands and lungs were shortly washed in PBS. Formalin-fixed paraffin embedded tissues were incubated for 3 h in 4% PFA (Electron Microscopy Sciences) and transferred through ascending dilutions of ethanol before embedment in paraffin. Fresh-frozen tissues were embedded in optimal cutting temperature compound (OCT; Tissue-Tek) on dry ice. Serial sections were obtained to ensure equal sampling of the examined specimens (5–7 µm trimming).

Immunofluorescence

Tissue sections were incubated overnight at 4°C with the following anti-mouse antibodies: FSP1 (Abcam; ab27957), αSMA (Sigma-Aldrich; F3777), Vimentin (Millipore; AB1620), PDGFRα (Santa Cruz; sc-101569), GFP (Rockland; 600-101-215), RFP (Rockland; 600-401-379), F4/80 (AbD Serotec; MCA497), Meca32 (BD; 550563) and cleaved caspase-3 (Abcam; Ab32042). Fluorescently conjugated secondary antibodies (Jackson ImmunoResearch Laboratories): Rhodamine Red-X–conjugated donkey anti-rabbit (711-295-152), Rhodamine Red-X–conjugated donkey anti-goat (705-295-147), Rhodamine Red-X–conjugated donkey anti-rat (712-295-153), Alexa Fluor 488–conjugated donkey anti-goat (705-545-147), and Alexa Fluor 488–conjugated goat anti-rabbit (111-545-144) were applied for 1 h at room temperature. Sections were mounted with DAPI Fluoromount-G (Southern Biotech; 0100-20).

Microscopy, image capture, and analysis

Slides were visualized and analyzed using Leica DM4000B microscope and digital camera (Leica DFC 360FX) using the Leica Application Suite software. Confocal images were captured for selected slides with a 63×/1.4 oil objective with Leica SP5 or SP8s or with ZEISS LSM 800 microscope. Quantitative

analyses were performed using ImageJ Software (National Institutes of Health).

Cleaved caspase-3 staining in Fig. 5 F and Meca32 staining in Fig. 6 F: images were captured with the Leica Aperio VERSA slide scanner and analyzed with the ImageScope software and Aperio Positive Pixel Count Algorithm. Analysis of human tissue sections was performed by a specialist pathologist (L. Leider-Trejo).

Cell lines

Met-1 mouse mammary gland carcinoma cells were a gift from J. Pollard (The University of Edinburgh, Scotland, UK). C18 primary mouse mammary gland carcinoma cells were prepared in our laboratory from fresh tumor tissue of MMTV-PyMT female mice (Sharon et al., 2015). The C166 endothelial cell line was purchased from the ATCC. All cell lines were routinely tested for mycoplasma using the EZ-PCR-Mycoplasma test kit (Biological Industries; 20-700-20).

Conditioned media

Met-1 and C18 cells were plated on 100-mm plastic plates and cultured with DMEM supplemented with 10% FCS, 1% penicillin-streptomycin, and 1% sodium-pyruvate (Biological Industries). When cells were at 80% confluency, plates were washed twice with PBS and fresh medium was applied. After 24 h, medium was collected, filtered through 0.2-µm filters under aseptic conditions, flash-frozen in liquid nitrogen and stored at −80°C. DMEM supplemented as above was used as control.

Normal fibroblasts and CAF cell cultures

Mammary glands and lungs were isolated from 6–8-wk-old FVB/n female mice. Single cell suspensions of mammary glands were prepared as previously described (Sharon et al., 2013). For dissociation of lung tissue, collagenase type II was substituted with trypsin (Biological Industries; 03-051-5B). Single cell suspensions were seeded on 6-well plates precoated with collagen (Corning; 354236). Cells were grown in DMEM media supplemented with 10% FCS (as above), and maintained at 37°C with 5% CO_2. Mammary and lung $EpCAM^-CD45^-$ CAFs were isolated by FACS from fresh tissue of mammary tumors or lungs bearing metastases of end-stage PyMT female mice. Cells were seeded on 24-well plates and cultured as above. All experiments were performed on low passage (p2-3) cells.

Resident and BM-derived CAF cell cultures

Resident and BM-derived CAFs were FACS sorted from mammary tumors of 12-wk-old PyMT-Col1α-YFP female mice and seeded on 24-well plates precoated with collagen (Corning; 354236). Cells were grown in DMEM media as above. Fibroblasts purity was confirmed by YFP expression using fluorescent microscopy. All experiments were performed on fresh, low passage (p2-3) cells.

BM-derived mesenchymal stem and progenitor cells cultures

BM cells were harvested aseptically from flushed femur and tibia of 6–8-wk-old Col1α-YFP female mice and cultured in complete Mesencult medium (Stem Cell Technologies; 05512) according to the manufacturer's protocol. All experiments were performed on fresh, low passage (p2-3) cells.

Total BM transplantations (BMT)

6-wk-old FVB/n, MMTV-PyMT, *Col1α*-DsRed/YFP, and PyMT;*Col1α*-DsRed/YFP female mice were lethally irradiated using an x-ray machine (160HF; Philips) at a total dose of 9 Gy. 24 h post-irradiation, mice were injected i.v. with 2.5×10^6 unfractionated BM cells harvested aseptically from flushed femur and tibia of age-matched FVB/n-GFP, MMTV-PyMT;GFP, *Col1α*-DsRed/YFP, or PyMT;*Col1α*-DsRed/YFP female mice. Following transplantation, mice received antibiotics for 4 wk in drinking water (Enrofloxacin; 0.2 mg/ml). To ensure radiation lethality, one mouse was irradiated without transplantation. To study the possible influence of the BMT procedure itself on tumor growth, transplanted mice were followed for weight and tumor development in comparison to age-matched control FVB/n and MMTV-PyMT mice. Chimerism was validated by immunofluorescent staining of BM smears from recipient mice. MMTV-PyMT;GFP and PyMT;*Col1α*-DsRed/YFP recipients were euthanized when mammary tumors reached 1.5 cm in diameter, according to Institutional Animal Care and Use Committee guidelines. FVB/n GFP and *Col1α*-DsRed/YFP recipients were sacrificed at the same time point.

In vivo Matrigel plug assays

2.7×10^5 resident CAFs or BM-derived CAFs in 100 µl PBS were mixed with 400 µl Growth Factor Reduced Matrigel (Corning; 356231) and injected into the right inguinal mammary gland of 8-wk-old FVB/n female mice. Control mice were injected with Matrigel mixed with PBS alone. 3 wk after injection, the plugs were dissected out and embedded in OCT for histological analysis.

Plug assay with siControl and siClusterin transfected fibroblasts

2.5×10^5 fibroblasts in 100 µl PBS (BM-derived CAFs transfected with siControl, BM-derived CAFs transfected with siClusterin, or resident CAFs) were mixed with 400 µl Growth Factor Reduced Matrigel (Corning; 356231) and additional siRNA, and injected into the right inguinal mammary gland of 8-wk-old FVB/n female mice. 1 wk after injection the plugs were dissected out and embedded in OCT for histological analysis.

Flow cytometry

Mammary glands and lungs

Mammary glands and lungs were isolated from mice. Single cell suspensions of mammary glands were prepared as we previously described (Sharon et al., 2013). For dissociation of lung tissue, collagenase type-II was substituted with trypsin (Biological Industries; 03–051-5B). Cells were stained using the following antibodies: anti-PDGFRα-PE (eBioscience; 12–1401-81), anti-EpCAM-APC (Miltany Biotec; 130–102-234), anti-CD45-PerCP-Cy5.5 (eBioscience; 45–0451-82), anti-CD45-PE-Cy7 (eBioscience; 25–0451-82), anti-Annexin V-Alexafluor 488 (Invitrogen; A13201), anti-CD34–FITC (eBioscience; 11–0341-82), and anti-αSMA-FITC (Sigma; F3777). For intracellular staining, cells were fixed and permeabilized with BD Cytofix/Cytoperm Plus kit according to the manufacturer's protocol. DAPI was used to exclude dead cells (Molecular Probes; D3571). Analysis or sorting was done with BD FACSAria II, BD FACSAria Fusion or CytoFLEX Flow Cy-

tometer (Beckman Coulter, Inc.). Data analysis was done with BD FACSDiva software (BD Biosciences), CytExpert 2.0 (Beckman Coulter, Inc.) or the Kaluza Flow Analysis software (Beckman Coulter, Inc.).

Peripheral blood (PB) and BM

Peripheral blood (PB) and BM were isolated from mice. For PB, RBCs were lysed using PharmLyse lysing buffer (BD; 555899). Cells were stained with anti-CD45-PerCP-Cy5.5 (eBioscience; 45–0451-82). DAPI was used to exclude dead cells. Analysis was performed with BD FACSAria II. Data analysis was done with BD FACSDiva software (BD Biosciences).

HSCs and MSCs for BM transplantation

BM cells were harvested aseptically from femur, tibia and iliac bones of 6–8-wk old Col1α- DsRed female mice and enriched for c-kit (CD117) using magnetic beads (Miltenyi Biotec; 130-091-224). The pellet cells were stained with the mouse Lineage Cell Detection Cocktail-FITC (Miltenyi Biotec; 130-092-613), anti–CD45-PerCP-Cy5.5 (eBioscience; 45-0451-82), anti-CD34-FITC (eBioscience; 11-0341-82), anti–Sca-1-APC (eBioscience; 17-5981-82). DAPI (Molecular probes; D3571) was used to exclude dead cells. Sorting was done with BD FACSAria II. Data analysis was done with BD FACSDiva software (BD Biosciences).

RNA isolation and qRT-PCR

Cells of interest pooled from at least three mice were collected into TRIzol LS reagent (Life Technologies; 10296-028) and RNA was isolated according to the manufacturer's instructions. Alternatively, for in vitro experiments, total RNA was isolated from cell pellets using PureLinkTM RNA Mini kit (Invitrogen; 12183018A). cDNA was reverse transcribed using iScript (Bio-Rad; 1708841) or qScript cDNA Synthesis kit (Quanta; 95047–100). qRT-PCR analyses were conducted using iTaq Universal SYBR Green Supermix (Bio-Rad; 172-5121) with the primers listed in Table 1.

In all analyses expression results were normalized to GAPDH and mGUS. RQ ($2^{-\Delta Ct}$) was calculated. Error bars represent SD or SEM as indicated.

Gene expression analysis

Total RNA was isolated from BM-derived and resident CAFs sorted from mammary tumors and lung bearing metastases in both BM transplantation systems and analyzed for the expression of 561 immune-related genes using the NanoString nCounter gene expression immunology panel (NanoString Technologies, Inc.). Data were analyzed according to the manufacturer's guidelines, and heat map presentation of differentially expressed genes of resident versus BM-derived CAFs in primary tumor and lungs bearing macrometastases was generated using Microsoft Excel software. The cutoff for presentation was differential expression of at least 1.5-fold (for mammary gland tumors) or 10-fold (for metastases bearing lungs) between resident and BM-derived fibroblasts. Expression of selected genes was validated by qRT-PCR. Venn diagrams were generated using the BioVenn (Hulsen et al., 2008).

Hierarchical clustering was generated using ClustVis (Metsalu and Vilo, 2015).

Table 1. **Primer sequences**

Gene symbol	Sequence (5′–3′)
Gapdh	F: TCTTGTGCAGTGCCAGCCT; R: CCAATACGG CCAAATCCGT
Acta2	F: AGCCAGTCGCTGTCAGGAA; R: CGAAGCCGG CCTTACAGA
Col1α	F: TGTGTTCCCTACTCAGCCGTCT; R: CTCGCTTCC GTACTCGAACG
S100A4	F: CACTTCCTCTCTCTTGGTCTGGTC; R: GTGGAA GGTGGACAATTACATC
Vimentin	F: TTTCTTCCCTGAACCTGAGAGAA; R: GTCCAT CTCTGGTCTCAACCGT
PDGFRα	F: GACTGGAAGCTTGGGGCTTA; R:GTCCCCATA GCTCCTGAGACCT
PTPRC	F: CAGAGACCACATATCATCCAGGTG; R: GCTTGG CTGCTGAATGTCTGA
F4/80	F: ACTGTCTGCTCAACCGTCAGGT; R: GGAATG GGAGCTAAGGTCAGTCT
Cdh1	F: ACACCGTAGTCAACGATCCTGA; R: GCCTCA AAATCCAAGCCCTT
Pecam1	F: CCACCAGAGACATGGAATACCA; R: CAACTT CATCCACTGGGGCTA
DsRed	F: GAAGCTGAAGGTGACCAAGG; R: TAGTCCTCG TTGTGGGAGGT
Clusterin	F: CGTCCAGGGAGTGAAGCACA; R: CCTAGTGTC CTCCAGAGCATCCT
FAP	F: TACGACCTTCAGAATGGGGAAT; R: AACAGG CGACCAGCATAGATACT
FSP1	F: CACTTCCTCTCTCTTGGTCTGGT; R: GTGGAA GGTGGACACAATTACAT
KRT19	F: GAGGACTTGCGCGACAAGAT; R: CGTGTTCTG TCTCAAACTTGGTTCT
PyMT	F: AAAGGTGGAAGCCATGCCTTA; R: AGCCGGTTC CTCCTAGATTCAT

HSC and MSC transplantations followed by intramammary tumor cells injection

HSCs and MSCs were isolated using magnetic beads and FACS as described above. 6-wk-old Col1α-YFP female mice were lethally irradiated using an x-ray machine (160HF; Philips) at a total dose of 9 Gy. 24 h after irradiation, mice were injected i.v. with 1.5×10^5 HSC fraction, with or without 6×10^3 MSC cells. Following transplantation, mice received antibiotics for 4 wk in drinking water (Enrofloxacin; 0.2 mg/ml). To ensure radiation lethality, one mouse was irradiated without transplantation. 2 wk following transplantation, 2×10^5 Met-1 cells were injected into the right inguinal mammary gland of the transplanted mice. An incision was made 0.5 cm medial to the gland to enable accurate intramammary injection. Cells were suspended in PBS and mixed 1:1 in volume with Growth Factor Reduced Matrigel (BD Biosciences) immediately before injection. Tumors were measured every 2–3 d with a caliper, and tumor volumes were calculated using the formula $X^2 \times Y \times 0.52$ (X = smaller diameter; Y = larger diameter). Tumor growth was measured for 24 d after injection. Mice were euthanized and tumors were weighed and either embedded in

OCT for histological analysis or digested into single cell suspension for FACS analysis.

Migration assay

Met1 (1×10^4) or C18 (1×10^4) cells were placed into the upper chamber of 24 Transwell inserts, with pore size of 8 µm. NMFs (1×10^4) or MSCs (1×10^4) were placed into the lower chamber. Following incubation for 24 h, the upper side of the upper chamber was scraped gently with cotton swabs to remove nonmigrating cells, fixed with methanol and stained with DAPI. Invading cells were imaged under a fluorescence microscope and quantified with ImageJ software.

Methylene blue viability assay

C166 endothelial cells were seeded in 96-well plates at 70% confluency. Following 6-h starvation, cells were incubated with conditioned media from PDGFRα$^+$ fibroblasts, PDGFRα$^-$ incubated with nontargeting siRNA or PDGFRα$^-$ incubated with Clusterin siRNA. 24 h later, cells were fixed in 0.5% glutaraldehyde, washed three times with DDW, and left to dry. Plates were stained with methylene blue solution (1% methylene blue in 0.1 M borate buffer, pH 8.5) at room temperature for 1 h. Plates were repeatedly washed with DDW and left to dry. Color was extracted with 0.1 M HCl by shaking at 37°C for 1 h. O.D. was measured at 630 nm.

Transfection of primary fibroblasts

FACS sorted fibroblasts were cultured in DMEM supplemented with 10% FCS. At 70% confluency, cells were transfected with Accell Delivery Media (GE Dharmacon; B-005000) supplemented with 1 µM Accell SMARTpool mouse Clusterin siRNA (GE Dharmacon; E-043966-00) or Accell Control Pool nontargeting siRNA (GE Dharmacon; D-001910-10) for 48 h. Accell SMARTpool contains a mixture of four siRNAs targeting one gene and provides extended duration of gene knockdown with only minimal effects on cell viability and the innate immune response. The efficiency of Clusterin siRNA knockdown was analyzed by qRT-PCR.

Statistical analyses

All statistical analyses were performed using GraphPad Prism software. Significance between two groups was calculated using Mann-Whitney test. All tests were two-tailed unless $n < 5$ in which case one-tailed Mann-Whitney U test was performed. P value of ≤0.05 was considered statistically significant for all datasets. Bar graphs represent mean and SD or mean and SEM across experimental repeats, as stated. All experiments were repeated at least twice.

Human data

RNA-seq and clinical data

Pre-processed and normalized RNA-seq gene expression in 10 diverse cancer types were obtained (see Fig. S5 E for details). Datasets were downloaded from TCGA.

Differential expression analysis

Differential expression was performed by comparing normal samples with primary tumors. Expression values are the $\log_2$ transformation of fragments per kilobase of transcript per million mapped reads. Differentially expressed genes were identified using an absolute fold-change cut-off of >1.5, and FDR corrected P values of <0.001, determined using two sample Student's t tests.

Breast cancer survival analysis

Clinical data of breast cancer patients were obtained from the TCGA and TCGA PANCAN database. Survival analysis was performed on $n = 1215$ patients, irrespective of the breast cancer types. Patient survival and status were derived from the columns '_TIME_TO_EVENT', overall survival in days, and '_EVENT', overall survival indicator (1 = death; 0 = censor).

Survival analysis was performed using the 'survival' package for R (version 2.38–3). Patients were divided into two groups of high and low expression levels using the median expression. Significance was determined using the χ^2 distribution and FDR-corrected for multiple testing. For specific breast cancer subtypes, patients were stratified by their expression of PR, ER, HER2, or lack of expression of all three and analyzed for survival as above with GraphPad.

PDGFRα expression in normal breast fibroblasts versus CAFs

PDGFRα-stained tissue sections from normal breast ($n = 2$) or tumors from patients with infiltrating ductal carcinoma ($n = 12$) were retrieved from the Human Protein Atlas, and analyzed by a specialist pathologist (L. Leider-Trejo). The percentage of PDGFRα$^+$ fibroblasts was quantified from the total number of fibroblasts for each section.

Online supplemental material

Fig. S1 shows gating strategy of FACS experiments presented in Fig. 1, immunofluorescence (IF) staining of αSMA and PDGFRα and percentage of PDGFRα$^{+/-}$ fibroblast at different stages of tumor progression. Fig. S2 shows IF of GFP in BM smear, co-staining of αSMA and GFP, gating strategy of FACS experiments presented in Fig. 2, and qRT-PCR analysis of resident and BM-derived fibroblasts. Fig. S3 shows qRT-PCR analysis of YFP$^+$ or YFP$^-$ cells, FACS analysis of PDGFRα in resident CAFs, and FACS analysis of YFP expression in peripheral blood and BM. Fig. S4 shows IF staining of Meca32 in plugs described in Fig. 4 and gating strategy of FACS experiments presented in Fig. 5. Fig. S5 shows Kaplan-Meier plots of breast cancer patients with high versus low expression of PDGFRα (for PR$^+$, ER$^+$, HER2$^+$, and triple-negative breast cancer). Table S1 details the TCGA datasets that were used in the analyses in Fig. 7 and in Fig. S5.

Acknowledgments

The authors would like to thank Dr. Irena Shur and the Sackler School of Medicine Interdepartmental Core Facility (SICF) for help with imaging, FACS, and PCR analyses and Elad Yana for graphical assistance.

This research was supported by grants to N. Erez from the European Research Council (ERC) under the European Union's Horizon 2020 research and innovation program (grant agreement no. 637069 MetCAF), from the Israel Science Foundation (grant no. 813/12), and The Israel Cancer Research Fund (Re-

search Career Development Award). This work was performed in partial fulfillment of the requirements for a PhD of Yael Raz, Sackler School of Medicine, Tel Aviv University.

The authors declare no competing financial interests.

Author contribution Y. Raz and N. Cohen conceived and carried out experiments, analyzed data and generated figures; O. Shani, L. Abramovitz, and S.V. Novitskiy carried out experiments; R.E. Bell performed bioinformatics analysis, L. Leider-Trejo, D. Grisaru, and M. Milyavsky were involved in data analysis and discussions; C. Levy and H.L. Moses contributed essential resources; N. Erez designed and supervised the study; N. Erez, Y. Raz, and N. Cohen wrote the manuscript.

Submitted: 3 May 2018
Revised: 5 September 2018
Accepted: 23 October 2018

References

Anderberg, C., and K. Pietras. 2009. On the origin of cancer-associated fibroblasts. *Cell Cycle.* 8:1461–1465. https://doi.org/10.4161/cc.8.10.8557

Anderberg, C., H. Li, L. Fredriksson, J. Andrae, C. Betsholtz, X. Li, U. Eriksson, and K. Pietras. 2009. Paracrine signaling by platelet-derived growth factor-CC promotes tumor growth by recruitment of cancer-associated fibroblasts. *Cancer Res.* 69:369–378. https://doi.org/10.1158/0008-5472.CAN-08-2724

Arina, A., C. Idel, E.M. Hyjek, M.L. Alegre, Y. Wang, V.P. Bindokas, R.R. Weichselbaum, and H. Schreiber. 2016. Tumor-associated fibroblasts predominantly come from local and not circulating precursors. *Proc. Natl. Acad. Sci. USA.* 113:7551–7556. https://doi.org/10.1073/pnas.1600363113

Barcellos-de-Souza, P., G. Comito, C. Pons-Segura, M.L. Taddei, V. Gori, V. Becherucci, F. Bambi, F. Margheri, A. Laurenzana, M. Del Rosso, and P. Chiarugi. 2016. Mesenchymal Stem Cells are Recruited and Activated into Carcinoma-Associated Fibroblasts by Prostate Cancer Microenvironment-Derived TGF-β1. *Stem Cells.* 34:2536–2547. https://doi.org/10.1002/stem.2412

Beer, T.M., S.J. Hotte, F. Saad, B. Alekseev, V. Matveev, A. Fléchon, G. Gravis, F. Joly, K.N. Chi, Z. Malik, et al. 2017. Custirsen (OGX-011) combined with cabazitaxel and prednisone versus cabazitaxel and prednisone alone in patients with metastatic castration-resistant prostate cancer previously treated with docetaxel (AFFINITY): a randomised, open-label, international, phase 3 trial. *Lancet Oncol.* 18:1532–1542. https://doi.org/10.1016/S1470-2045(17)30605-8

Bergfeld, S.A., and Y.A. DeClerck. 2010. Bone marrow-derived mesenchymal stem cells and the tumor microenvironment. *Cancer Metastasis Rev.* 29:249–261. https://doi.org/10.1007/s10555-010-9222-7

Bochet, L., C. Lehuédé, S. Dauvillier, Y.Y. Wang, B. Dirat, V. Laurent, C. Dray, R. Guiet, I. Maridonneau-Parini, S. Le Gonidec, et al. 2013. Adipocyte-derived fibroblasts promote tumor progression and contribute to the desmoplastic reaction in breast cancer. *Cancer Res.* 73:5657–5668. https://doi.org/10.1158/0008-5472.CAN-13-0530

Borowsky, A.D., R. Namba, L.J. Young, K.W. Hunter, J.G. Hodgson, C.G. Tepper, E.T. McGoldrick, W.J. Muller, R.D. Cardiff, and J.P. Gregg. 2005. Syngeneic mouse mammary carcinoma cell lines: two closely related cell lines with divergent metastatic behavior. *Clin. Exp. Metastasis.* 22:47–59. https://doi.org/10.1007/s10585-005-2908-5

Broekema, M., M.C. Harmsen, M.J. van Luyn, J.A. Koerts, A.H. Petersen, T.G. van Kooten, H. van Goor, G. Navis, and E.R. Popa. 2007. Bone marrow-derived myofibroblasts contribute to the renal interstitial myofibroblast population and produce procollagen I after ischemia/reperfusion in rats. *J. Am. Soc. Nephrol.* 18:165–175. https://doi.org/10.1681/ASN.2005070730

Bucala, R., L.A. Spiegel, J. Chesney, M. Hogan, and A. Cerami. 1994. Circulating fibrocytes define a new leukocyte subpopulation that mediates tissue repair. *Mol. Med.* 1:71–81.

Cao, Y. 2013. Multifarious functions of PDGFs and PDGFRs in tumor growth and metastasis. *Trends Mol. Med.* 19:460–473. https://doi.org/10.1016/j.molmed.2013.05.002

Carvalho, I., F. Milanezi, A. Martins, R.M. Reis, and F. Schmitt. 2005. Overexpression of platelet-derived growth factor receptor alpha in breast cancer is associated with tumour progression. *Breast Cancer Res.* 7:R788–R795. https://doi.org/10.1186/bcr1304

Cohen, N., O. Shani, Y. Raz, Y. Sharon, D. Hoffman, L. Abramovitz, and N. Erez. 2017. Fibroblasts drive an immunosuppressive and growth-promoting microenvironment in breast cancer via secretion of Chitinase 3-like 1. *Oncogene.* 36:4457–4468. https://doi.org/10.1038/onc.2017.65

Direkze, N.C., S.J. Forbes, M. Brittan, T. Hunt, R. Jeffery, S.L. Preston, R. Poulsom, K. Hodivala-Dilke, M.R. Alison, and N.A. Wright. 2003. Multiple organ engraftment by bone-marrow-derived myofibroblasts and fibroblasts in bone-marrow-transplanted mice. *Stem Cells.* 21:514–520. https://doi.org/10.1634/stemcells.21-5-514

Direkze, N.C., K. Hodivala-Dilke, R. Jeffery, T. Hunt, R. Poulsom, D. Oukrif, M.R. Alison, and N.A. Wright. 2004. Bone marrow contribution to tumor-associated myofibroblasts and fibroblasts. *Cancer Res.* 64:8492–8495. https://doi.org/10.1158/0008-5472.CAN-04-1708

Driskell, R.R., B.M. Lichtenberger, E. Hoste, K. Kretzschmar, B.D. Simons, M. Charalambous, S.R. Ferron, Y. Herault, G. Pavlovic, A.C. Ferguson-Smith, and F.M. Watt. 2013. Distinct fibroblast lineages determine dermal architecture in skin development and repair. *Nature.* 504:277–281. https://doi.org/10.1038/nature12783

Erez, N., M. Truitt, P. Olson, S.T. Arron, and D. Hanahan. 2010. Cancer-Associated Fibroblasts Are Activated in Incipient Neoplasia to Orchestrate Tumor-Promoting Inflammation in an NF-kappaB-Dependent Manner. *Cancer Cell.* 17:135–147. https://doi.org/10.1016/j.ccr.2009.12.041

Erez, N., S. Glanz, Y. Raz, C. Avivi, and I. Barshack. 2013. Cancer associated fibroblasts express pro-inflammatory factors in human breast and ovarian tumors. *Biochem. Biophys. Res. Commun.* 437:397–402. https://doi.org/10.1016/j.bbrc.2013.06.089

Erler, J.T., and V.M. Weaver. 2009. Three-dimensional context regulation of metastasis. *Clin. Exp. Metastasis.* 26:35–49. https://doi.org/10.1007/s10585-008-9209-8

Fathke, C., L. Wilson, J. Hutter, V. Kapoor, A. Smith, A. Hocking, and F. Isik. 2004. Contribution of bone marrow-derived cells to skin: collagen deposition and wound repair. *Stem Cells.* 22:812–822. https://doi.org/10.1634/stemcells.22-5-812

Fu, Y., Y. Lai, Q. Wang, X. Liu, W. He, H. Zhang, C. Fan, and G. Yang. 2013. Overexpression of clusterin promotes angiogenesis via the vascular endothelial growth factor in primary ovarian cancer. *Mol. Med. Rep.* 7:1726–1732. https://doi.org/10.3892/mmr.2013.1436

Gascard, P., and T.D. Tlsty. 2016. Carcinoma-associated fibroblasts: orchestrating the composition of malignancy. *Genes Dev.* 30:1002–1019. https://doi.org/10.1101/gad.279737.116

Goetz, J.G., S. Minguet, I. Navarro-Lérida, J.J. Lazcano, R. Samaniego, E. Calvo, M. Tello, T. Osteso-Ibáñez, T. Pellinen, A. Echarri, et al. 2011. Biomechanical remodeling of the microenvironment by stromal caveolin-1 favors tumor invasion and metastasis. *Cell.* 146:148–163. https://doi.org/10.1016/j.cell.2011.05.040

Hanahan, D., and L.M. Coussens. 2012. Accessories to the crime: functions of cells recruited to the tumor microenvironment. *Cancer Cell.* 21:309–322. https://doi.org/10.1016/j.ccr.2012.02.022

Hulsen, T., J. de Vlieg, and W. Alkema. 2008. BioVenn - a web application for the comparison and visualization of biological lists using area-proportional Venn diagrams. *BMC Genomics.* 9:488. https://doi.org/10.1186/1471-2164-9-488

Jiang, X., Z. Kalajzic, P. Maye, A. Braut, J. Bellizzi, M. Mina, and D.W. Rowe. 2005. Histological analysis of GFP expression in murine bone. *J. Histochem. Cytochem.* 53:593–602. https://doi.org/10.1369/jhc.4A6401.2005

Kalluri, R. 2016. The biology and function of fibroblasts in cancer. *Nat. Rev. Cancer.* 16:582–598. https://doi.org/10.1038/nrc.2016.73

Kalluri, R., and M. Zeisberg. 2006. Fibroblasts in cancer. *Nat. Rev. Cancer.* 6:392–401. https://doi.org/10.1038/nrc1877

Karnoub, A.E., A.B. Dash, A.P. Vo, A. Sullivan, M.W. Brooks, G.W. Bell, A.L. Richardson, K. Polyak, R. Tubo, and R.A. Weinberg. 2007. Mesenchymal stem cells within tumour stroma promote breast cancer metastasis. *Nature.* 449:557–563. https://doi.org/10.1038/nature06188

Koltai, T. 2014. Clusterin: a key player in cancer chemoresistance and its inhibition. *OncoTargets Ther.* 7:447–456. https://doi.org/10.2147/OTT.S58622

Kususda, Y., H. Miyake, M.E. Gleave, and M. Fujisawa. 2012. Clusterin inhibition using OGX-011 synergistically enhances antitumour activity of sorafenib in a human renal cell carcinoma model. *Br. J. Cancer.* 106:1945–1952. https://doi.org/10.1038/bjc.2012.209

Lamoureux, F., M. Baud'huin, B. Ory, R. Guiho, A. Zoubeidi, M. Gleave, D. Heymann, and F. Rédini. 2014. Clusterin inhibition using OGX-011 synergistically enhances zoledronic acid activity in osteosarcoma. *Oncotarget.* 5:7805–7819. https://doi.org/10.18632/oncotarget.2308

LeBleu, V.S., G. Taduri, J. O'Connell, Y. Teng, V.G. Cooke, C. Woda, H. Sugimoto, and R. Kalluri. 2013. Origin and function of myofibroblasts in kidney fibrosis. *Nat. Med.* 19:1047–1053. https://doi.org/10.1038/nm.3218

Levental, K.R., H. Yu, L. Kass, J.N. Lakins, M. Egeblad, J.T. Erler, S.F. Fong, K. Csiszar, A. Giaccia, W. Weninger, et al. 2009. Matrix crosslinking forces tumor progression by enhancing integrin signaling. *Cell.* 139:891–906. https://doi.org/10.1016/j.cell.2009.10.027

López-Ruano, G., R. Prieto-Bermejo, T.L. Ramos, L. San-Segundo, L.I. Sánchez-Abarca, F. Sánchez-Guijo, J.A. Pérez-Simón, J. Sánchez-Yagüe, M. Llanillo, and Á. Hernández-Hernández. 2015. PTPN13 and β-Catenin Regulate the Quiescence of Hematopoietic Stem Cells and Their Interaction with the Bone Marrow Niche. *Stem Cell Reports.* 5:516–531. https://doi.org/10.1016/j.stemcr.2015.08.003

Meleshina, A.V., E.I. Cherkasova, M.V. Shirmanova, N.V. Klementieva, E.V. Kiseleva, L.B. Snopova, N.N. Prodanets, and E.V. Zagaynova. 2015. Influence of mesenchymal stem cells on metastasis development in mice in vivo. *Stem Cell Res. Ther.* 6:15. https://doi.org/10.1186/s13287-015-0003-7

Metsalu, T., and J. Vilo. 2015. ClustVis: a web tool for visualizing clustering of multivariate data using Principal Component Analysis and heatmap. *Nucleic Acids Res.* 43(W1):W566–70. https://doi.org/10.1093/nar/gkv468

Mi, Z., S.D. Bhattacharya, V.M. Kim, H. Guo, L.J. Talbot, and P.C. Kuo. 2011. Osteopontin promotes CCL5-mesenchymal stromal cell-mediated breast cancer metastasis. *Carcinogenesis.* 32:477–487. https://doi.org/10.1093/carcin/bgr009

Mishra, P.J., P.J. Mishra, R. Humeniuk, D.J. Medina, G. Alexe, J.P. Mesirov, S. Ganesan, J.W. Glod, and D. Banerjee. 2008. Carcinoma-associated fibroblast-like differentiation of human mesenchymal stem cells. *Cancer Res.* 68:4331–4339. https://doi.org/10.1158/0008-5472.CAN-08-0943

Mishra, P.J., P.J. Mishra, J.W. Glod, and D. Banerjee. 2009. Mesenchymal stem cells: flip side of the coin. *Cancer Res.* 69:1255–1258. https://doi.org/10.1158/0008-5472.CAN-08-3562

Öhlund, D., E. Elyada, and D. Tuveson. 2014. Fibroblast heterogeneity in the cancer wound. *J. Exp. Med.* 211:1503–1523. https://doi.org/10.1084/jem.20140692

Orimo, A., and R.A. Weinberg. 2007. Heterogeneity of stromal fibroblasts in tumors. *Cancer Biol. Ther.* 6:618–619. https://doi.org/10.4161/cbt.6.4.4255

Östman, A. 2017. PDGF receptors in tumor stroma: Biological effects and associations with prognosis and response to treatment. *Adv. Drug Deliv. Rev.* 121:117–123. https://doi.org/10.1016/j.addr.2017.09.022

Pallangyo, C.K., P.K. Ziegler, and F.R. Greten. 2015. IKKβ acts as a tumor suppressor in cancer-associated fibroblasts during intestinal tumorigenesis. *J. Exp. Med.* 212:2253–2266. https://doi.org/10.1084/jem.20150576

Peng, Y., Z. Li, P. Yang, I.P. Newton, H. Ren, L. Zhang, H. Wu, and Z. Li. 2014. Direct contacts with colon cancer cells regulate the differentiation of bone marrow mesenchymal stem cells into tumor associated fibroblasts. *Biochem. Biophys. Res. Commun.* 451:68–73. https://doi.org/10.1016/j.bbrc.2014.07.074

Pietras, K., J. Pahler, G. Bergers, and D. Hanahan. 2008. Functions of paracrine PDGF signaling in the proangiogenic tumor stroma revealed by pharmacological targeting. *PLoS Med.* 5:e19. https://doi.org/10.1371/journal.pmed.0050019

Quante, M., S.P. Tu, H. Tomita, T. Gonda, S.S. Wang, S. Takashi, G.H. Baik, W. Shibata, B. Diprete, K.S. Betz, et al. 2011. Bone marrow-derived myofibroblasts contribute to the mesenchymal stem cell niche and promote tumor growth. *Cancer Cell.* 19:257–272. https://doi.org/10.1016/j.ccr.2011.01.020

Redondo, M., E. Villar, J. Torres-Muñoz, T. Tellez, M. Morell, and C.K. Petito. 2000. Overexpression of clusterin in human breast carcinoma. *Am. J. Pathol.* 157:393–399. https://doi.org/10.1016/S0002-9440(10)64552-X

Ruffell, B., D. Chang-Strachan, V. Chan, A. Rosenbusch, C.M. Ho, N. Pryer, D. Daniel, E.S. Hwang, H.S. Rugo, and L.M. Coussens. 2014. Macrophage IL-10 blocks CD8+ T cell-dependent responses to chemotherapy by suppressing IL-12 expression in intratumoral dendritic cells. *Cancer Cell.* 26:623–637. https://doi.org/10.1016/j.ccell.2014.09.006

Servais, C., and N. Erez. 2013. From sentinel cells to inflammatory culprits: cancer-associated fibroblasts in tumour-related inflammation. *J. Pathol.* 229:198–207. https://doi.org/10.1002/path.4103

Shangguan, L., X. Ti, U. Krause, B. Hai, Y. Zhao, Z. Yang, and F. Liu. 2012. Inhibition of TGF-β/Smad signaling by BAMBI blocks differentiation of human mesenchymal stem cells to carcinoma-associated fibroblasts and abolishes their protumor effects. *Stem Cells.* 30:2810–2819. https://doi.org/10.1002/stem.1251

Shao, Z.M., M. Nguyen, and S.H. Barsky. 2000. Human breast carcinoma desmoplasia is PDGF initiated. *Oncogene.* 19:4337–4345. https://doi.org/10.1038/sj.onc.1203785

Sharon, Y., L. Alon, S. Glanz, C. Servais, and N. Erez. 2013. Isolation of normal and cancer-associated fibroblasts from fresh tissues by Fluorescence Activated Cell Sorting (FACS). *J. Vis. Exp.* (71):e4425.

Sharon, Y., Y. Raz, N. Cohen, A. Ben-Shmuel, H. Schwartz, T. Geiger, and N. Erez. 2015. Tumor-derived osteopontin reprograms normal mammary fibroblasts to promote inflammation and tumor growth in breast cancer. *Cancer Res.* 75:963–973. https://doi.org/10.1158/0008-5472.CAN-14-1990

Spaeth, E.L., A.M. Labaff, B.P. Toole, A. Klopp, M. Andreeff, and F.C. Marini. 2013. Mesenchymal CD44 expression contributes to the acquisition of an activated fibroblast phenotype via TWIST activation in the tumor microenvironment. *Cancer Res.* 73:5347–5359. https://doi.org/10.1158/0008-5472.CAN-13-0087

Sugimoto, H., T.M. Mundel, M.W. Kieran, and R. Kalluri. 2006. Identification of fibroblast heterogeneity in the tumor microenvironment. *Cancer Biol. Ther.* 5:1640–1646. https://doi.org/10.4161/cbt.5.12.3354

Tang, Y., F. Liu, C. Zheng, S. Sun, and Y. Jiang. 2012. Knockdown of clusterin sensitizes pancreatic cancer cells to gemcitabine chemotherapy by ERK1/2 inactivation. *J. Exp. Clin. Cancer Res.* 31:73. https://doi.org/10.1186/1756-9966-31-73

Tellez, T., M. Garcia-Aranda, and M. Redondo. 2016. The Role of Clusterin in Carcinogenesis and its Potential Utility as Therapeutic Target. *Curr. Med. Chem.* 23:4297–4308. https://doi.org/10.2174/0929867323666161024150540

Tsujino, T., I. Seshimo, H. Yamamoto, C.Y. Ngan, K. Ezumi, I. Takemasa, M. Ikeda, M. Sekimoto, N. Matsuura, and M. Monden. 2007. Stromal myofibroblasts predict disease recurrence for colorectal cancer. *Clinical cancer research: an official journal of the American Association for Cancer Research* 13:2082-2090.

Uhlén, M., L. Fagerberg, B.M. Hallström, C. Lindskog, P. Oksvold, A. Mardinoglu, Å. Sivertsson, C. Kampf, E. Sjöstedt, A. Asplund, et al. 2015. Proteomics. Tissue-based map of the human proteome. *Science.* 347:1260419. https://doi.org/10.1126/science.1260419

Wang, Y., A.S. Brodsky, J. Xiong, M.L. Lopresti, D. Yang, and M.B. Resnick. 2018. Stromal Clusterin Expression Predicts Therapeutic Response to Neoadjuvant Chemotherapy in Triple Negative Breast Cancer. *Clin. Breast Cancer.* 18:e373–e379. https://doi.org/10.1016/j.clbc.2017.08.007

Yom, C.K., H.Y. Woo, S.Y. Min, S.Y. Kang, and H.S. Kim. 2009. Clusterin overexpression and relapse-free survival in breast cancer. *Anticancer Res.* 29:3909–3912.

Yu, P.F., Y. Huang, C.L. Xu, L.Y. Lin, Y.Y. Han, W.H. Sun, G.H. Hu, A.B. Rabson, Y. Wang, and Y.F. Shi. 2017. Downregulation of CXCL12 in mesenchymal stromal cells by TGFβ promotes breast cancer metastasis. *Oncogene.* 36:840–849. https://doi.org/10.1038/onc.2016.252